Chitosan-graft-Poly(trichlorovinylsilane) Polymers: Synthesis, Characterization, Antibacterial Susceptibility and Dye Adsorption Studies

Anthony Udukhomo Awode

Submitted to the
Institute of Graduate Studies and Research
in partial fulfillment of the requirements for the degree of

Doctor of Philosophy
in
Chemistry

Eastern Mediterranean University
January 2020
Gazimağusa, North Cyprus

Approval of the Institute of Graduate Studies and Research

Prof. Dr. Ali Hakan Ulusoy
Director

I certify that this thesis satisfies all the requirements as a thesis for the degree of Doctor of Philosophy in Chemistry.

Prof. Dr. İzzet Sakallı
Acting Chair, Department of Chemistry

We certify that we have read this thesis and that in our opinion it is fully adequate in scope and quality as a thesis for the degree of Doctor of Philosophy in Chemistry.

Prof. Dr. Mustafa Gazi
Supervisor

Examining Committee

1. Prof. Dr. Murat Ateş
2. Prof. Dr. Mustafa Gazi
3. Prof. Dr. Okan Sirkecioğlu
4. Prof. Dr. Elvan Yılmaz
5. Assoc. Prof. Dr. Akeem Oladipo

ABSTRACT

In this study, chitosan-*grafted*-trichlorovinylsilane (CT–*g*–VTCS) film is produced and elucidated by X-ray diffraction (XRD), Fourier transform infrared spectroscopy (FTIR), Scanning electron microscopy (SEM) and Energy dispersive X-ray (EDX). The SEM micrograph of exhibited refine structure with rough surface. The CT–*g*–VTCS antibacterial action was assayed using the agar diffusion and broth dilution approach. Obtained results herein pointed out that CT–*g*–VTCS exhibited increased water solubility (67 mg/mL) when compared with chitosan (CT) film (2.6 mg/mL). CT–*g*–VTCS exhibited improved antibacterial action against *S. aureus, E. coli, Kleb spp., E. faecalis* and Methicillin-resistant *Staphylococcus aureus (MRSA)* (minimum inhibitory concentration (MIC) = 0.078 – 0.156 mg/mL and minimum bactericidal concentration (MBC) = 12.5 – 3.12 mg/mL) higher than the precursor CT film. Contrary to most quaternized chitosan derivatives, the CT–*g*–VTCS was processed via a simple and easy route and showed comparatively high antibacterial efficiency. Studies from the time-kill assessment revealed that 5 mg/mL CT–*g*–VTCS exposed to the bacteria cells is copious to give a ~0.08 $\log_{10}$ reduction (>99.9% kill rate) within 24 h.

Vinyltrichlorosilanechitosan-graft-polyacrylamide (VCSCT-g-PAAm) hydrogel was also synthesized. From the results obtained, hydrogels with varying molar ratios of VCSCT-g-PAAm all formed within 13 min. The incorporation of polyacrylamide onto vinyltricholosilane–chitosan backbone enhanced the hydrogel physical and chemical properties in terms of strength, swelling capacity, adsorptivity and antimicrobial activity. The VCSCT-g-PAAm hydrogel interacted with methylene blue (MB) dye

solution at different mass-liquid ratio, pH and temperature. The amount of MB dye removal was estimated using UV-Vis spectrophotometer at an optical density of λ_{max}= 665nm. The MB dye removal was most effective at pH 12 with about 98% removal at 50^{o}C. The hydrogel was characterized by Fourier Transform Infrared Spectroscopy (FTIR) and other physicochemical parameters. Experimental data obtained for the adsorbent-MB dye pair suited the Langmuir, Freundlich and pH-dependent Langmiur-Freundlich adsorption isotherms. Calculated values for ΔH^{o}, ΔS^{o}, ΔG^{o} were -2.72kJ/mol, 16.72J/mol K and 7.73kJ/mol correspondingly. Further studies revealed high swelling ratio in basic solution with about 1,179% swellability. Investigations showed that VCSCT-g-PAAm hydrogel exhibited a high percentage killing against *S. aureus and E. coli*, more than 99.9% kill rate after 24 hr contact with *S.aureus* and *E.coli*, this can contribute immensely in biomedical application and beneficial in waste water treatment.

Keywords: Chitosan, Trichlorovinylsilane, Antibacterial, Adsorption, Methylene blue.

ÖZ

Bu çalışmada, kitosan triklorovinilsilan aşılı kopolimer (CT-g-VTCS) filmi üretildi ve X-ışını kırınımı (XRD), Fourier dönüşümü kızılötesi spektroskopisi (FTIR), Taramalı elektron mikroskopisi (SEM) ve Enerji dağıtıcı x-ışını (EDX) ile analiz edildi. CT-g-VTCS' nin SEM mikrografisi, çıkıntı yüzeye sahip rafine bir yapı göstermiştir. CT-g-VTCS' nin antibakteriyel etkisi, agar difüzyonu ve sıvı bakteri büyüme ortamı seyreltme yaklaşımı kullanılarak analiz edildi. Burada elde edilen sonuçlar, CT-g-VTCS' nin, çapraz bağlı kitosan (CT) film (2.6 mg / mL) ile karşılaştırıldığında artırılmış suda çözünürlük (67 mg / mL) sergilediğine dikkat çekmiştir. Ayrıca, CT-g-VTCS tarafından, *S. aureus, E. coli, Kleb* spp., *E. faecalis* ve Metisiline dirençli *Staphylococcus aureus*'a (MRSA) (minimum inhibitör konsantrasyon (MIC) = 0.078 - 0.156 mg / mL ve minimum bakterisidal konsantrasyon (MBC) =12.5 - 3.12 mg / mL) karşı öncü CT filme kıyasla geliştirilmiş bir antibakteriyel etki sergilediği görülmüştür. Çoğu kuaternize kitosan türevinin aksine, CT-g-VTCS basit ve kolay bir yolla üretildi ve nispeten yüksek antibakteriyel verimlilik gösterdi. Bakterilerin zamana karşı öldürme değerlendirmesinden elde edilen sonuçlar, bakteri hücrelerine uygulanan 5 mg / mL CT-g-VTCS' nin 24 saat içinde ~ 0.08 log10 azalma (>% 99.9 öldürme oranı) sağladığını ortaya koymuştur.

Viniltriklorosilankitosan-poliakrilamid aşılı (VCSCT-g-PAAm) hidrojel de sentezlenmiştir. Elde edilen sonuçlara göre, değişen molar oranlara sahip olan VCSCT-g-PAAm hidrojellerin hepsinin 13 dakika içinde oluştuğu gözlemlenmiştir. Poliakrilamidin viniltriklorosilan-kitosan omurgası üzerine dahil edilmesi, mukavemet, şişme kapasitesi, adsorptivite ve antimikrobiyal aktivite açısından

hidrojelin fiziksel ve kimyasal özelliklerini arttırdığı görülmüştür. VCSCT-g-PAAm hidrojeli, farklı kütle-sıvı oranı, pH ve sıcaklıkta metilen mavisi (MB) boya çözeltisi ile etkileşime girdirilerek boya giderimi denenmiştir. MB boya giderim miktarı, λmax = 665nm optik yoğunlukta UV-Vis spektrofotometre kullanılarak tahmin edildi. MB boyasının giderimi en çok %98'lik oranla pH 12'de 50 ° C'de gerçekleşmiştir. Hidrojel, Fourier Dönüşümü Kızılötesi Spektroskopisi (FTIR) ve diğer fizikokimyasal parametreler ile karakterize edildi. Adsorban-MB boya çifti için elde edilen deneysel veriler, Langmuir, Freundlich ve pH'a bağlı Langmiur-Freundlich adsorpsiyon izotermlerine uygundur. ΔH^o, ΔS^o, ΔG^o için hesaplanan değerler sırasıyla -2.72kJ / mol, 16.72J / mol K ve 7.73kJ / mol olarak bulunmuştur. Diğer çalışmalar, bazik çözeltide yaklaşık % 1.179 şişebilirlik ile yüksek şişme oranını ortaya çıkardı. Araştırmalar, VCSCT-g-PAAm hidrojelinin *Staphylococcus aureus (S.aureus)* ve *Escherichia coli*'ye (*E.coli*) karşı antibakteriyel aktivitesi olduğunu gösterdi, bu bulgular biyomedikal uygulamalara son derece katkıda bulunabilir ve atık su arıtımında faydalı olabilir.

Anahtar Kelimeler: Kitosan, Triklorovinilsilan, Antibakteriyel, Adsorpsiyon, Metilen mavisi

DEDICATION

This thesis is dedicated to the king of kings, the Lord of Lords, the savior of my soul, Jesus Christ.

ACKNOWLEDGEMENTS

I am most grateful to God almighty for the grace and strength bestowed upon me to complete this work. All through my difficulties He was leading and guiding me.

My profound appreciation to Prof. Dr. Mustafa Gazi, my thesis supervisor for the assistance rendered throughout the process of this thesis. I will forever remain grateful to Prof. Dr. Osman Yilmaz for his valuable advice and support. A big thank you to Assoc. Prof. Dr. Akeem Oladipo, for his innumerable contribution to the success of this thesis Many thanks to Prof. Dr. Elvan Yilmaz for her countless advice. My sincere appreciation to the entire staff of faculty of medicine EMU for your love and support.

Many thanks to the University of Jos, Plateau state, Nigeria for availing me the opportunity and continued support all through my study at EMU. To the management and entire staff of chemistry department University of Jos, thank you for your prayers and support.

To my wonderful friend and colleagues at EMU, Ayodeji Ifebajo, Edith Ahaka, Kola Azalok, Naizi, Namik, Faisal, Abdullah, and everyone, thank you all for your support.

I will forever remain grateful to my sweetheart and loving wife, Mrs. Chidinma Awode.. To my lovely precious angels, Cara and Nora, thank you for enduring my absence these past years. My deepest appreciation to my father, chief Francis Awode, Sir & Lady Eddy Agwuegbo, Charles Awode, the entire Awode's and Agwuegbo's family. I love you all.

TABLE OF CONTENTS

LIST OF TABLES

LIST OF FIGURES

LIST OF SYMBOLS AND ABBREVIATIONS

a_R	Redlich-Peterson Isotherm constant (1/mg)
a_S	Sips Isotherm model constant (L/mg)
b	Langmuir Isotherm constant (dm3/mg)
BA	Blood Agar
BET	Brunauer-Emmett-Teller
C_e	Concentration at equilibrium (mg/L)
C_i	Initial Concentration (mg/L)
CT	Chitosan
CT-g-VTCS	Chitosan graft poly(trichlorovinylsilane)
CT-g-VTCSB	Crosslinked Chitosan graft poly(trichlorovinylsilane)
E.coli	Escherichia Coli
EDX	Energy Dispersed X-ray Spectroscopy
FTIR	Fourier-Transform Infrared
Kleb. Spp.	Klebsiella Species
K_{YN}	Rate Constant (min^{-1})
MB	Methylene Blue
MBC	Minimum Bactericidal Concentration
MG	Malachite Green
MHA	Muller Hinton Agar
MHB	Muller Hinton Broth
MIC	Minimum Inhibitory Concentration
MRSA	Methicillin Resistant Staphylococcus Aureus
PFO	Pseudo First Order
PSO	Pseudo Second Order
q_e	Equilibrium Adsorption Efficiency (mg/g)

q_m or q_{TH}	Maximum Adsorption Efficiency (mg/g)
R^2	Correlation Coefficient Value
RB	Rhodamine B
S.aureus	Staphylococcus aureus
VCS-CT-g-PAAm	Vinyltrichloro-chitosan-graft-polyacrylamide
VTCS	Trichlorovinylsilane or Vinyltrichlorosilane
XRD	X-ray Diffraction
λ_{max}	Maximum Wavelength

Chapter 1

INTRODUCTION

In this study, trichlorovinylsilane (VTCS) was used to modify the surface of chitosan (CT). VTCS is currently attracting increasing attention because of its high solubility in water and organic solvents (Komata et al. 2016), and its oxidative chlorine with rapid biocidal activity against a wide range of microbes (Shin et al. 2013). Also, Sluszny et al. (2001) reported that the mechanical and thermal stability of a poly (vinyl chloride)–based semi-IPN film was significantly improved after the introduction of vinyl silane content.

Hence, considering the beneficial properties of the VTCS and chitosan, it is expected that grafting VTCS onto chitosan backbone would result in film with enhanced water solubility, mechanically stable and rapid antibacterial performance compared to the non-modified CT. Unlike most reported quaternized chitosan derivatives, the fabrication of Chitosan-g-poly(trichlorovinylsilane) polymer (CT-g-VTCS) is through an easy and simple route. The incorporation of silicon into chitosan matrix will provides some strength to the material.

The second objective of this study was to use trichlorovinylsilane grafted chitosan (CT-g-VTCS) to crosslink acrylamide and produce a hydrogel with high swelling/adsorption capacity and good antibacterial property. No information or work

using trichlorovinylsilane modified chitosan and acrylamide has been reported in the literature.

1.1 Chitin and Chitosan

Chitosan, poly[β-(1 –4)-2-amino-2-deoxy-D-glucose] is the product obtained from the N-deacetylation of chitin with a strong alkali. Figure 1 and 2 shows the structures of chitin and chitosan respectively.

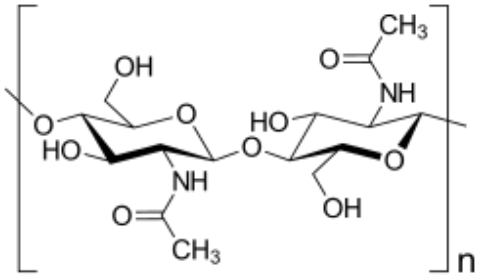

Figure 1: Structure of Chitin

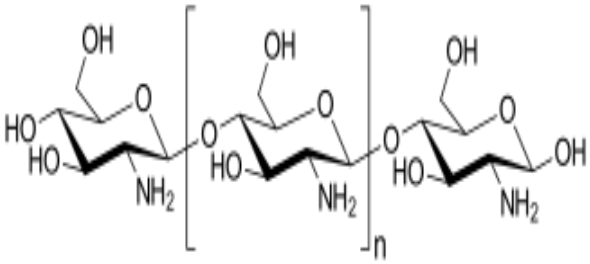

Figure 2: Structure of Chitosan

Chitosan is a very well-known versatile biopolymer (Kaur and Dhillon 2014; Yilmaz 2004) with properties like biocompatibility, biodegradability, affinity towards toxic and radioactive metals, being antibacterial, and remarkable affinity towards proteins and enzymes (Casal et al. 2006). Affinity towards proteins had been used in vast variety of applications. For example, it has been used in selective adsorption of some proteins (Casal et al. 2006) from dairy products. On the other hand, chitosan has been

used as the antifouling agent against biofouling of proteins (Boributh et al.2009; Correia et al. 2013) in some other applications.

Chitin, poly [β-(1=4)-2-acetamido-2-deoxy-D-glucose] is found in the exoskeleton of insects and crutaceans and also in the cell wall of yeast and fungi (Yeul 2012). Chitin is a hard, white, inelastic naturally abundant mucopolysacharide rich in nitrogen and a by-product of fishery business only second to cellulose in terms of natural abundance (Islam 2017).

Chitin and chitosan has similar structure to that of cellulose and consists of several hundreds to more than thousand β-(1-4) linked D-glucose units (Bhuiyan 2014). The hydroxyl group of the C-2 position in cellulose (Figure3) has been exchanged by an acetamide group. The deacetylation of chitin is always never complete and there will still remain some acetamide groups in chitosan (deacetylated chitin).

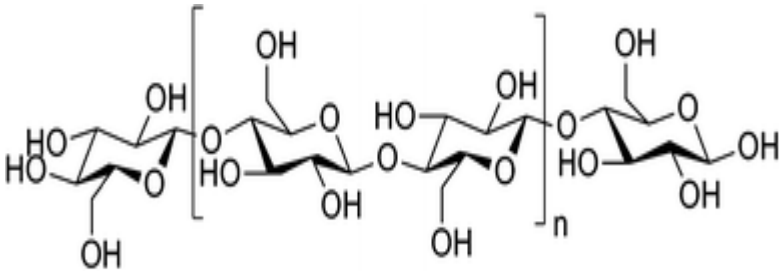

Figure 3: Structure of Cellulose

There is still about 5-8% of nitrogen contained in chitin and chitosan unlike in cellulose, this presence of nitrogen makes chitin to carry acetylated amine group and chitosan to have primary aliphatic amine groups thereby making them to exhibit similar amines reactions (Kurita 2001). The presence of primary and secondary hydroxyl group on each repeat unit and amine group on each deacetylated unit makes

chitosan more reactive than chitin. The presence of these reactive groups on chitosan makes it subject to chemical modifications and the various uses to which it is put to.

The repeated treatment process of chitin using 40-45% NAOH at 160 ^{o}C results in about 98% degree of deacetylation and never 100%. The degree of acetylation (DD) ranges from 56-99% depending on the method employed. Chitosan with a DD of 85% is usually used in most reactions because of its solubility in acetic acid (No and Meyers 1995).

1.1.1 Uses of Chitin and Chitosan

Chitosan and chitin has extensive uses in the field of biomedical engineering such as tissue engineering, artificial kidney membrane, wound healing/wound dressing, artificial skin, bone damage repair, articular cartilage, bio-artificial liver (BAL), nerve repair, artificial tendon, burn treatment, blood anticoagulation, blood vessel tubes, umbilical hernia treatment, absorbable sutures, drug delivery systems, antimicrobial/antifungal, catheter manufacture (chitosan-heparin) and cancer treatment (Islam, S et al. 2017). Chitosan based hydrogel has also shown a lot of potential in heavy metal and dye removal in waste water treatment (Vinh et al. 2018).

Physicochemical properties of chitin and chitosan that enables its usefulness in biomedical applications are DD, distribution of acetyl groups, molecular weight and viscosity. These physicochemical characteristics of chitosan and chitin are tied to their properties such as biocompatibility, antioxidant, hemostatic, mucoadhesion, analgesic, anticholesterolic and biodegradability (Aranaz et al. 2009).

1.2 Trichlorovinylsilane, Properties and Uses

VTCS has the structural formular 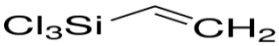 with a molecular weight of 161.49g. It has a vapour pressure of 60mmHg at 23ºC, a boiling point of 90 ºC and melting point of -95 ºC. It is highly soluble in water, has a density of 1.27g/ml at 25 ºC and usually stored between 2-8 ºC. Trichlorovinylsilane may react with lithium-tert-butyl and 1,3-enynes to yield isomeric silacyclobutanes and silacyclobutenes respectively.

1.3 Grafting

Grafting has been the focus of much research of late, because it offers a method which can impart an array of functional groups to a polymer backbone. The process of graft co-polymerization can be initiated through a variety of ways, such as high energy radiation, chemical treatment, photo irradiation etc. Grafting methods are broadly organized into three groups (i) ionic polymerization (ii) free radical (iii) addition and condensation polymerization.

(A) Free radical grafting: In free radical grafting through chemical process, the initiators produce free radicals which are transferred to the substrate and reacts with the monomer producing graft co-polymer (Bhattacharya and Misra 2004). Free radicals can generally be generated through indirect or direct methods. A good example of indirect generation of free radical is through the redox reaction of R^{n+}/H_2O_2, persulphates (Misra et al. 1980 ; Prasanth and Tharanathan 2003).

$$Fe^{2+} + H_2O_2 \rightarrow Fe^{3+} + OH^- + OH^{\bullet}$$

$$Fe^{2+} + -O_3S - OO - SO_3^- \rightarrow Fe^{3+} + SO_4^{2-} + SO_4^{-\bullet}$$

The active species from this decomposition of H_2O_2 and persulphate by Fe^{2+} are $OH^{\bullet}$ and $SO_4^{-\bullet}$. These active species can then react directly with the polymer backbone.

$$\text{Polymer} + SO_4^{-\bullet} \rightarrow Polymer^{\bullet} + HSO_4^-$$

Sometimes $SO_4^{-\bullet}$ reacts with water to produce $OH^{\bullet}$ which in turn reacts with the polymer backbone to produce free radicals on the polymer.

$$SO_4^{-\bullet} + H_2O \rightarrow HSO_4^- + OH^{\bullet}$$

A general mechanism of free radical graft polymerization involves initiation (start), propagation (growth/transfer) and termination (stop) of the polymer growing chain.

(i) Initiation: The first step of the initiation process involves the decomposition of the initiator molecule into free radicals.

$$R_2 \rightarrow 2R^{\bullet}$$

The second step of the initiation process is the activation of the monomer molecule by the active radical leading to chain initiation.

$$R^{\bullet} + M \rightarrow RM^{\bullet}$$

(ii) Propagation: This stage involves propagation of the active polymer chain.

$$RM^{\bullet} + nM \rightarrow R_iM_n^{\bullet}$$

The next step involves the transfer of the active site to another polymer chain.

$$R_iM_n^{\bullet} + LK \rightarrow R_iM_nL + K^{\bullet}$$

(iii) Termination: The final step involves the termination of the growing/grafted polymer chain, it can be either through combination or disproportionation reaction.

$$R_iM_n^{\bullet} + R_iM_m^{\bullet} \rightarrow R_iM_{n+m} \qquad \text{combination}$$

$$R_iM_n^{\bullet} + R_iM_m^{\bullet} \rightarrow R_iM_n + R_iM_m \qquad \text{disproportionation}$$

Graft copolymer that are randomly distributed can be synthesized through three routes (i) grafting to (ii) grafting from (iii) grafting through (Gitty and Masha 2014). Fig 3 illustrates these routes.

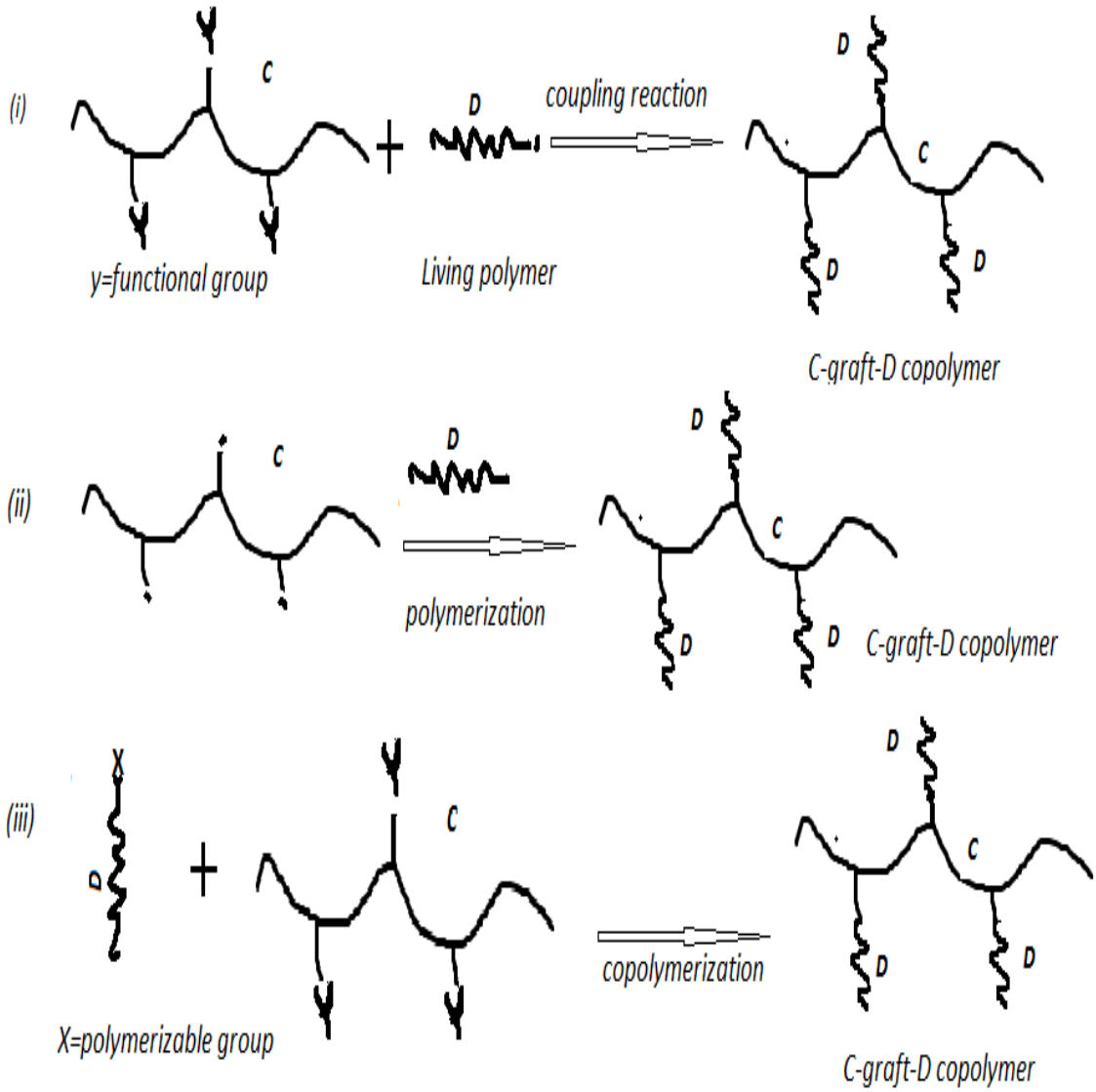

Figure 4: General Mechanism of Graft Polymerization.

Fenton reagent (hydroxides and Fe^{2+}) also produce free radicals in the form of $OH^{\bullet}$ which then reacts with the polymer backbone. Other examples of initiators that produce free radicals are benzoyl peroxide (BPO) and azoisobutyronitrile (AIBN), although their efficiency is low during grafting.

(B) Ionic grafting: The useful initiators for ionic grafting are organometallic compounds, sodium naphthalenide and alkali metal suspensions in a Lewis base liquid.

Carbonium ions are formed when alkyl aluminium reacts with the polymer backbone in the halide form (ACI). A cationic mechanism is responsible for this reaction.

$$ACl + R_3Al \rightarrow A + R_3AlCl^-$$

$$A^+ + M \rightarrow AM^+$$

Other cationic catalyst that can be used is BF_3.

The reaction can also proceed through anionic mechanism. Methoxide of alkali metals or sodium-ammonia forms alkoxide of polymer (PO-Na^+) this in turn reacts with the monomer forming graft co-polymer (Bhattacharya and Misra 2004).

$$P - OH + NaOR \rightarrow PO^-Na^+ + ROH$$

$$PO^- + M - POM^-M^- \rightarrow graft\ co - polymer$$

(C) Grafting by condensation and addition reactions: Addition and condensation reactions grafting is not a popular method of grafting and hardly studied. An example of graft condensation reaction is polyethylene glycol monmethyl ether on poly(methacrylic acid-co-methyl methacrylate) (Negahi Shirazi et al 2011). The addition reaction of hexamethylene di-isocyanate and 1, 2 diethyl alcohol is another example.

1.3.1 Antibacterial Polymers

Antibacterial polymers are a category of polymers that exhibit the ability to inhibit the growth or kill bacteria (Ikeda et al 1984). Polymers with antibacterial potency can be grouped into nonstimulated and potential antibacterial polymers (Li et al. 2018). Polymers that have nonstimulated antibacterial property possess inherent configuration in their design that are effective against bacteria cells. Chitosan and chitin falls under these category of natural biopolymer with inherent antibacterial activity (Kong et al 2010).

Potential antibacterial polymers are classified as polymers that can be transformed into efficient antibacterial agents when subjected to certain treatment, like subjection to light (Li et al 2018). The crosslinking/grafting of one polymer with another is another method for the synthesis of potential antibacterial polymer, for example photodynamic poly(2-hydroxyethyl methacrylate-co-methyl methacrylate) P(HEMA-co-MAA) copolymers crosslinked by porphyrin and photodynamic PHEMA-based hydrogel are effective against bacteria cells (Parsons et al 2009; Halpenny et al. 2009) .

1.3.2 Antibacterial Activity of Chitosan and Chitosan Hydrogels

A growing number of research has been directed towards biomaterials asserting antibacterial activity (Guler et al. 2016; Ozseker and Akkaya 2016; Gritsch et al. 2018). Amidst these biomaterials, chitosan (CT, the deacetylated derivative of chitin) is generally used in biomedical and pharmaceutical applications (Gritsch et al. 2018; Yan et al. 2019; Chylińsk et al. 2019), due to its appealing biological peculiarity such as cytocompatibility, moderate biocidal activity and low toxicity (Chylińsk et al. 2019). Chitosan exact biocidal mechanisms are still unknown (Alqahtani et al. 2019). Nonetheless, the intracellular percolation is among the frequently reported theories in that the protonated chitosan (amino groups at the C-2 position) at pH < 6.5 electrostatically binds to the negatively charged moieties on the microbe cells (Alqahtani et al. 2019; Kong et al. 2010; Rabea et al. 2003). Earlier studies disclosed that the biocidal properties of chitosan are strongly dependent on its molecular weight, charge density and degree of deacetylation (Chylińsk et al. 2019; Kong et al. 2010; Rabea et al. 2003; Verlee et al. 2017). Likewise, it is important to mention that it is difficult for chitosan to be directly dissolved in neutral water and alkaline pH due to the linear aggregation of its chain molecules and the configuration to crystallinity (Abureesh et al. 2016). Consequently, chitosan is ordinarily dissolved in dilute acids

(such as formic acid, acetic acid, etc.) and these acids carry high health hazard for mammalian cells, therefore there is a serious restraint of its potential biomedical utilizations. Thus, concerted study is being focused on improving the water solubility and antimicrobial effects of chitosan, mainly by chemical functionalization of the molecule (Rabea et al. 2003; Verlee et al. 2017; Abureesh et al. 2016; Bakshi et al. 2018; Chen et al. 2016). To overcome these impediment, researchers have focused their attention on the fabrication of quaternary derivatives of chitosan. In comparison with chitosan, the derivatives with quaternary ammonium groups manifested greater antibacterial activity (Chen et al. 2016). Derivatives of chitosan that are water-soluble has been reportedly synthesized through various schemes. Studies of Chen and coworkers (Chen et al. 2016) for example, published that by inserting quaternary ammonium compound onto the backbone of chitosan (N-substituted), improved its water solubility (from ~2.6 to 113.3 mg/mL) and antibacterial action towards *E. coli* (from ~6 to 15 mm); notwithstanding, biocompatibility property is compromised. Again, Wen et al. (2015) and Guo et al. (2014) illustrated that the chemical alterations of CT by quaternary phosphonium compounds through its NH_2 groups enhanced its water-solubility and charge density, which afterwards improved the antibacterial activity. Contrary to the chitosan N-substituted derivatives, Dang and co-workers (2018) examined the activity of N-acetylethylenediamine groups grafted to C-3,6–OH of chitosan (AEDMCS) across six bacteria. The findings established AEDMCS displayed reduced thermostability, permissible cytotoxicity and exigently greater antibacterial activity than the pristine chitosan. Remarkably, the various steps involved in the preparation of most CT derivatives as previously reported are time engrossing and complex.

Ye et al. (2016) also reported antibacterial activity of maleilated chitosan and thiol derivatised hyaluronan hydrogel against Staphylococcus aureus (*S. aureus*) and *E. coli* with killing percentage of 86.4± 4.9% and 63.0±4.4% respectively. Ferfera-Harrar et al (2014) incorporated Montmorillonite (MMT) into chitosan-g-poly(acrylamide) to produce a superabsorbent polymer with swelling, thermal and antibacterial properties. They established that the swelling equilibrium ratio in water increases with increasing MMT loading until 5wt%. They also reported moderate antibacterial activity of the superabsorbent hydrogel in acidic medium, where the sensitivity of *E. coli* was lower when compared to *S.aureus.* Rohindra and co-workers (2004) investigated the activity of crosslinked chitosan hydrogel with glutaraldehyde. They obtained a maximum swelling ratio of about 950% under different temperature and pH. There was no report on the antibacterial activity of the prepared hydrogel.

1.3.3 Waste Water Treatment and Dye Adsorption

It is estimated that over 280,000 tonnes per year of various dyes are discharged into water bodies globally (Ogugbue and Sawidis 2011). A good percentage of these dyes are not effectively treated before release into waste water (Gita et. al 2017). These dyes poses a huge environmental challenge to the biodiversity and the usability of these water bodies. Microbial contamination in water is on the increase due to exponential growth in human population leading to increased production of sewage, medical and industrial waste (Jabeen 2011). The need to rid water bodies of both textile effluent (dyes) and microbial contamination is of utmost necessity as water is becoming a scare commodity.

Various methods have been developed for the treatment of waste water, these include physical water treatment, biological water treatment, chemical treatment, and sludge treatment (online 2018). These methods are effective but they take time and usually

involve high energy demand leading to higher cost. An extensive review of the advantages and disadvantages of these method has been published (Hameed 2009; Salleh et. al 2011). Sorption technology which is a hybrid of physical and chemical treatment method has gained prominence as a result of the low cost of operation and its effectiveness (Bhatti et. al 2012; Bhatti and Safa 2012; Mittal et. al 2010).

Diverse techniques utilizing low-cost adsorbents have been successfully advanced for dye removal (Daraei et. al 2013; Noreen et. al 2013). In recent years, hydrogel-based materials have been widely studied because of their beneficial properties and have been used in water treatment, bio-sensing, biomedical engineering, agriculture and horticulture (soil water conservation and agro-chemical slow release), drug delivery, and sanitary products (disposable diapers and female pads) (Puoci et. al 2008; Kosemund et. al 2009). Hydrogels are polymeric materials with three dimensional networks retaining a large quantity of water within their structures (Buenger et. al 2012; Holback et. al 2011).

Hydrogel made purely from synthetic materials and metal ions have their drawbacks, this is due to their environmental impact and toxicity to living cells when used as antibacterial agent (Grade et. al 20). Moreover nanoparticle based hydrogels development has been restricted due to their physical and chemical instability (Li et. al 2018). Formulation of antimicrobial hydrogel without the incorporation of heavy metal nanoparticle is therefore imperative to overcome their cytotoxicity.

To address these drawbacks, researchers have focused their attention on the synthesis of polysaccharide based hydrogel with high water retaining capacity and improved antibacterial activity. Asgharzadehahmadi et al. (2013) prepared hydrogel based on

polyacrylamide and carboxymethyl containing magnesium oxide nanoparticle with antibacterial activity against Escherichia coli (*E. coli*) a gram negative food pathogenic bacteria. They stated that the zone of inhibition against *E.coli* was three times less without the addition of magnesium oxide nanoparticle. Ye et.al (2016) also synthesized a hydrogel with maleilated chitosan and thiol derivatised hyaluronan using a facile one-pot approach via Michael addition reaction.

1.3.3.1 Adsorption Isotherms

1.3.3.1.1 Langmuir Isotherm

The Langmuir isotherm describes a monolayer sorption onto a homogenous surface and is given by equation (1) (Langmuir 1916).

$$\frac{1}{q_e} = \frac{1}{q_m} + \frac{1}{K_L q_m C_e} \quad (1)$$

The most important feature of the Langmuir isotherm R_L known as the dimensionless constant separation factor helps to foretell if an adsorption system is favorable or unfavorable and is given by equation (2). Adsorption System is favorable when $(0 < R_L < 1)$, Unfavorable $(R_L > 1)$, linear $(R_L = 1)$, irreversible $(R_L = 0)$,

$$R_L = \frac{1}{1 + K_L C_0} \quad (2)$$

Where C_e is the (mg/dm^3) is the dye concentration at equilibrium in solution. q_e (mg/g) is the dye concentration onto the adsorbent. q_m (mg/g) is the MB concentration onto the adsorbent when monolayer forms. C_0 (mg/dm^3) is the initial dye concentration. K_L is the Langmuir constant (dm^3/mg).

1.3.3.1.2 Freundlich Isotherm

The Freundlich isotherm describes adsorption on a surface that is heterogeneous with an exponential distribution of active sites (Freundlich 1907). It is given by equation (3).

$$ln\, q_e = lnK_F + \frac{1}{n} lnC_e \quad (3)$$

where K_F (dm^3/mg) and n are Freundlich constants, derived from the plot of lnq_e versus lnC_e. The variables K_F and *1/n* are linked to adsorption capacity and the adsorption intensity of the system. The size of the expression (*1/n*) offers an insight of the favorability of the adsorbent/adsorbate systems (Levan and Vermeulen 1981).

1.3.3.1.3 Redlich-Peterson Isotherm

A mixture of the Langmuir and Freundlich isotherm represents the Redlich-Peterson isotherm. The parameters on the numerator is from the Langmuir isotherm and approaches the Henry region at infinite dilution (Davoundinejad and Gharbanian 2013). It is a three parameter isotherm incorporating Langmuir and Freundlich equations, consequently the adsorption mechanism is a blend and monolayer adsorption is not followed (Brouers and Al-Musawi 2015).

The expression for the model is as follows:

$$q_e = \frac{AC_e}{1+BC_e^{\beta}} \tag{4}$$

Where *A* is Redlich-Peterson isotherm constant (dm^3/g), *B* is constant (dm^3/mg), β is exponent that lies between 0 and 1, C_e is equilibrium liquid-phase concentration of the adsorbent (mg/dm^3), and q_e is equilibrium adsorbate loading on the adsorbent (mg/g). The equation is reduced to the Freundlich equation at high liquid-phase concentration.

$$q_e = \frac{AC_e^{1-\beta}}{B} \tag{5}$$

where $A/B = K_F$ and $(1-\beta) = 1/n$ for the Freundlich isotherm model.

When $\beta = 1$, this is reduced to Langmuir equation with $b = B$ (Langmuir adsorption constant (dm^3 /mg which is connected to the energy of adsorption).

$A = bq_{ml}$ where q_{ml} is Langmuir maximum adsorption capacity of the adsorbent (mg/g); when $\beta = 0$, the Henry's equation is obtained with $1/(1+b)$ denoting Henry's constant.

Redlich-Peterson isotherm can be expressed in the linear form as (Kiseler 1958):

$$ln\frac{C_e}{q_e} = \beta\, ln\, C_e - ln\, A \quad (6)$$

Plotting $ln\ (C_e/q_e)$ against $ln\ C_e$ allows the calculation of Redlich-Peterson constants, with β as slope and A intercept (Ng et al. 2002, Wu et al. 2010).

1.3.3.1.4 Sips Isotherm

The Sips isotherm is a combined expression of Langmuir and Freundlich isotherms which is given by the expression in (7). It represents a system in which one adsorbed molecule likely fills more than one active site (Sreńscek- Nazzal et al. 2015).

$$q_e = \frac{q_m K_s C_e^{\beta_s}}{1+K_s C_e^{\beta_s}} \quad (7)$$

Where K_s is the model constant (dm^3/mg), q_m is the Sips maximum adsorption capacity (mg/g), and β is the Sips exponent outlining heterogeneity. The linearized expression of Sips isotherm is given as (8) :

$$\beta_e lnC_e = -ln\left(\frac{K_s}{q_e}\right) + lnK_s \quad (8)$$

The limitation of Freundlich model can be avoided by using this model which is suitable for forecasting adsorption on heterogeneous surfaces when adsorbate concentration is increased (Travis and Etnier 1981). This model is reduced to Freundlich model at low adsorbate concentration and at high adsorbate concentration the Langmuir model is predicted. The terms of Sips model isotherm are dependent on changes in temperature, concentration and pH (Chen 2012; Elmorsi 2011; Foo and Hammed 2009).

1.3.3.2 Adsorption Kinetics

Adsorption of MB dye onto VCS-CT-g-PAAm hydrogel was performed by extracting, taking the absorbance of the sample and analyzing the results at a given time interval of 30, 60, 120, 240, 360, 1440 min. The kinetic experiments were performed with an

initial MB dye concentration of 20 mg/dm^3 and at a temperature of 300 K. The following equation was used in calculating the amount of dye adsorbed at time *t*.

$$q_t = \frac{(C_0 - C_t)V}{M} \quad (9)$$

where C_0 (mg/dm^3) and C_t (mg/dm^3) are the initial and time *t* concentrations of dye respectively. *M* (g) is the mass of hydrogel and *V* (dm^3) is the volume of solution used.

1.3.3.2.1 Pseudo First Order (PFO)

This is the most extensively used kinetic model to predict dye adsorption onto adsorbent. The kinetic model is represented by the following equation (10):

$$\frac{dq}{dt} = k_1(q_e - q_t) \quad (10)$$

where k_1 (min^{-1}) is the rate constant of the first order adsorption, q_t (mg/g) adsorbed amount at time *t* (min) and q_e (mg/g) adsorped amount at equilibrium. Applying integration at these given conditions $q_t = 0$ at $t = 0$ and $q_t = q_t$ at $t = t$ gives the following equation(11):

$$log(q_e - q_t) = log\, q_e - \left(\frac{k_1}{2.303}\right) t \quad (11)$$

The absorption rate k1 can be calculated from a plot of $log(q_e - q_t)$ verses *t*.

1.3.3.2.2 Pseudo Second Order (PSO)

The second order kinetics can be represented by the following equation (Ho and Mckay, 1999):

$$\frac{dq}{dt} = k_2(q_e - q_t)^2 \quad (12)$$

integrating the above equation under the following conditions $q_t = 0$ at $t = 0$ and $q_t = q_t$ at $t = t$ gives equation (13).

$$\frac{t}{q_t} = \frac{1}{k_2 q_e^2} + \frac{t}{q_e} \quad (13)$$

The rate constant k_2 (g/mg min) and q_e can be gotten from the intercept and slope when a plot of t/q_t verses *t* is made.

1.3.3.2.3. Elovich Kinetic Model

The activation, deactivation energy, surface diffusion and mass of a system is predicted by this model. An assumption is made that as the amount of adsorbed solute increases the rate of adsorption of solute decreases exponentially (Kajjumba et al 2018). The Elovich model equation is represented below:

$$\frac{dq_t}{dt} = \alpha \exp^{-\beta q_t} \tag{14}$$

As $q_t \approx 0$, $dq_t/dt \approx \alpha$ which is the initial adsorption rate (mg/g.min), and β is desorption constant. The Elovich model can be linearized after integrating and applying the limits for $t\ (0, t)$ and $q_t\ (0, q_t)$.

$$q_t = \frac{1}{\beta} ln\left[t + \frac{1}{\alpha\beta}\right] - \frac{1}{\beta} ln(\alpha\beta) \tag{15}$$

As the system approaches equilibrium $t \gg 1/\alpha\beta$, therefore equation (15) changes into:

$$q_t = \frac{1}{\beta} ln[\alpha\beta] + \frac{1}{\beta} lnt \tag{16}$$

The type of adsorption on the heterogeneous surface of the adsorbent can be identified by a plot of q_t against t, and tells if its chemisorption or not (Kajjumba et al. 2018).

1.3.3.2.4 Boyd Kinetic Model

Boyd model is useful in determining the rate controlling step or slow step in an adsorption activity. The information obtained from the graph of Boyd plot gives an indication of the kind of mechanism involved in the adsorption process. If the straight line on the plot passes through the origin then the particle diffusion mechanism is obtainable, but if the straight line doesn't pass through the origin then the film diffusion or bulk mass transport mechanism is obtainable (Elkady et. al 2016). The Boyd kinetic model is represented by the expression in equation (17).

$$F = 1 - \left(\frac{6}{\pi^2}\right) \exp(-B_t) \tag{17}$$

Where B_t is the function F that represents the fraction of adsorbed solute at different times t.

$$F = \frac{q_t}{q_\alpha} \tag{18}$$

Where q_t (mg/g) is the amount adsorbed at time t and q_α stands for the amount adsorbed at infinite time. Replacing $F = \frac{q_t}{q_\alpha}$ into equation 18, the expression is then written as:

$$B_t = -0.4978 - ln\left(1 - \frac{qt}{q\alpha}\right). \tag{19}$$

1.3.4 Chitosan Hydrogels in Dye Adsorption

Several chitosan hydrogels have been synthesized for the removal of various dyes and heavy metals in waste water treatment. A number of studies have utilized the abundant natural biopolymer CT in combination with other synthetic polymers. A study by Al-Mubaddel et al. (2015) synthesized chitosan polyacrylonitrile (CS/PAN) hydrogel for the adsorption of rhodamine B (RB) in aqueous solution, and had an adsorption capacity of 21.90 mg/g. Peng and co-workers (2015) studied the adsorption capacity of chitosan-halloysite nanotubes (HNTs/CS) hydrogel for the removal of methylene blue (MB) and malachite green (MG) from waste water with an adsorption capacity of 75.37 mg/g and 276.9 mg/g achieved respectively. Jin and Bai (2002) were able to synthesize chitosan-poly(vinylalcohol) (PVA-CS) hydrogel and used it for the adsorption studies of Pb^{2+}, an adsorption capacity of 2 mg/g was obtained.

Another study carried out by Ma et al. (2017) used chitosan-polyacrylamide (CS/PAM) hydrogel for the adsorption of Cd^{2+}, Cu^{2+} and Pb^{2+}, an adsorption capacity of 86, 99.4, 138.4 mg/g was recorded respectively. Chatterjee et al. (2009) synthesized chitosan-cetyl trimethyl ammonium bromide (CTAB-CS) hydrogel and used it for the adsorption of congo red, 352.5 mg/g was gotten as the adsorption capacity. Adsorption study by Zhao and Mitomo (2008) using carboxylmethyl cellulose chitosan (CM

cellulose/CS) hydrogel to adsorb Cu^{2+}, obtained 169.4 mg/g as the adsorption capacity of the hydrogel. A sodium alginate-water soluble chitosan (NaAlg/WSC) hydrogel was synthesized by You et al. (2015) and was used for the adsorption of heavy metals ions, acidic and basic gas.

Chapter 2

EXPERIMENTAL

2.1 Materials

All chemical reagents are analytical grade (> 98.5%), and distilled water was used in all experiments as a solvent. Vinyltrichlorosilane, sodium bisulfite and chitosan with a deacetylation degree of 85 % and molecular weight of 400,000 g/mol, acrylamide, N',N' isomethylacrylamide, benzaldehyde, Methylene blue (MB) and ammonium persulfite were purchased from Sigma–Aldrich (St. Louis, USA). All other solvents such as acetone, acetic acid, hydrochloric acid, methanol and ethanol were purchased from Merck (Darmstadt, Germany). Blood agar, Muller-Hinton Agar (MHA) and Mueller-Hinton broth (MHB) were obtained from Merck. The *E. coli* (ATCC-CRM-8739TM), Kleb spp. (ATCC 4352), *E. faecalis* (ATCC 29212), *S. aureus* (ATCC-CRM-6538TM) and Methicillin-resistant *S.aureus.*

2.2 Grafting

2.2.1 Grafting of Trichlorovinylsilane onto Chitosan Backbone

The CT-g-VTCS derivatives were synthesized as shown in Figure4. The preparation procedure contains two different pathways; specifically, the heterogeneous grafting of excess VTCS onto chitosan backbone and the homogeneous grafting of VTCS onto N-protected chitosan in the presence of sodium persulfate initiator. For details, 1 g CT was firstly dispersed in 1% glacial acetic acid (100 mL) and stirred for 6 h at room temperature to obtain a homogeneous solution. To ensure that VTCS reacts selectively with the OH position of chitosan backbone, the NH_2 position was protected as

described in (Gazi and Sayeh 2012). In order to protect amino groups, (1.0 g) sample was placed in ethanol (10 mL) and 4 g benzaldehyde was introduced to this mixture. The reaction was carried out for 12 h at room temperature. The product was filtered and washed several times with ethanol and dried at 40°C overnight. To de-protect the amine group of chitosan, 1.2 g of the product was wetted with 12.5 mL of water for 1 h and 50 mL of hydrochloric acid (0.5 M) was added to the mixture and stirred (500 rpm) at room temperature overnight. The product was filtered and washed several times with acetone, ethanol, and water, respectively and dried at 40°C.

Afterwards, 1 mL of VTCS in ethanol/water solution (25 ml, v/v = 98/2) was prepared. 4 mL VTCS (0.2 mol/L) solution was then introduced into the N-protected chitosan solution in the presence of a predetermined amount of sodium persulfate initiator ($Na_2S_2O_8$) in a three-necked round bottom flask. The mixture was allowed to react for 12 h in the presence of nitrogen gas over an oil bath at 60 °C. Finally, the product was casted on a petri dish; then precipitated in 3:2 ethanol–methanol mixture (200 mL) and vacuum dried at 60 °C to obtain water-soluble CT-g-VTCS as shown in Figure5 (path A). In contrast, a densely crosslinked chitosan-graft-poly(trichlorovinylsilane) was obtained when an excess of VTCS (10 mL) was introduced into the CT solution. The obtained product was then precipitated and purified as described above; then dried overnight and named as CT-g-VTCSB (path B).

2.2.2 Grafting of Acrylamide onto Trichlorovinylsilane-Chitosan Backbone

4 g medium molecular weight chitosan was weighed into a bottle, 10 mL of vinyltrichlorosilane was added and allowed to soak the chitosan for 3 days. After complete soaking and interaction with chitosan, the bottle was opened and excess fumes of VTCS allowed to escape. The VCS-CT was properly stored in a corked container.

50 mL 2.5% acetic acid was added into a conical flask containing 0.5 g of VCS-CT, this was allowed to stir overnight until complete dissolution. 10 mL of the VCS-CT solution was used in the preparation of the hydrogel by adding varying amount of acrylamide (0.9 g, 0.7 g, 0.5 g, 0.3 g), 0.05g N'N-methylbisacrylamide (crosslinker) and 0.05 g ammonium persulphate (initiator). The reaction was carried out at 70-80 ^{0}C until gel was formed.

Finally, the product was washed several times with distilled water and acetone and then dried at room temperature until constant weight was obtained.

2.2.3 Calculation of Percent Grafting

The percent grafting can be calculated for both homogenous and heterogeneous reactions using the equation below.

$$Grafting\ (\%) = \frac{copolymer\ (g) - chitosan(g)}{chitosan\ (g)} \times 100$$

2.3 Characterization

2.3.1 Fourier Transform Infrared Spectrophotometry (FTIR)

A Perkin-Elmer FTIR-8700 spectrophotometer was used to characterize the functional groups in the samples in the range of 4000–500 cm^{-1}.

2.3.2 X-ray Diffraction (XRD)

Powder XRD (X-ray diffraction) patterns were recorded using a D-8 Advance diffractometer (Bruker-AXS, Germany) operated at 40 kV, 30 mA, step size of 2" and Cu Kα radiation (λ=1.5417 Å). The crystalline phases of the samples were matched and identified using standard JCPDS files. The nitrogen isotherms were determined at −196 °C on an Autosorb analyzer (QuantaChrome, USA), and the specifc surface areas and pores distribution were evaluated from the nitrogen isotherm using the Brunauer–Emmett–Teller (BET) and Brunauer–Joyner–Halenda (BJH) equations, respectively.

2.3.3 Scanning Electron Microscopy (SEM) and Energy Dispersive X-ray (EDX)

Scanning electron microscopy (SEM, JEOL, Japan) fitted with an energy dispersive X-ray (EDX) was utilized to characterize the morphology and the chemical compositions of as-synthesized samples.

2.4 Solubility of CT-g-VTCS and CT

The solubility of dried CT and CT-g-VTCS in distilled water, acetic acid and phosphate-buffered solution (pH 7.4) at room temperature was investigated. In brief, 0.1 g of each sample was suspended in 10 mL liquid media and stirred for 5 h at 25 °C. The undissolved solids were then passed through a filter membrane of pore size 0.45 µm and dried in the oven at 50 °C until constant weight was attained. The solubility (S%) was calculated according to Eq.20 where w represents the weight of undissolved sample (g):

$$S\% = \frac{\mathbf{0.1}-\boldsymbol{w}\mathbf{0.1}}{\mathbf{0.1}} \times 100 \quad (20)$$

2.5 Determination of Point of Zero Charge (PZC)

The salt addition method was used in measuring PZC as reported by Mahmood et al. (2011). A weighed mass of hydrogel (0.025 g) and 0.01 M NaCl (25 mL) were mixed in 250 mL flask. The pH of the mixtures were adjusted between 2, 3, 4, 5, 6, 7, 8, 9, 10 using 0.1 M HCl or 0.1 M NaOH. The flask were agitated on a shaker for 24 h , after which the final pH was measured. The ΔpH values is plotted against the initial pH values. The initial pH at which ΔpH is zero was taken to be the PZC (Mahmood et al. 2011; Tan et. al 2008; Anderson and Rubin 1981).

2.6 Dye Adsorption Experiments

2.6.1 Preparation of Calibration Curve

The calibration curve for the adsorption test was made by dissolving pre-weighed amount of MB in distilled water. 2, 4, 6, 8, 10, 20 and 100 mg/L were prepared from

a stock solution of 250 mg/L concentration. The various concentrations of MB solutions were adjusted to pH 9 and the absorbance reading of each concentration read using a UV spectrophotometer. A graph of absorbance vs concentration (mg/L) was then plotted and used to estimate the amount of MB adsorbed onto VCS-CT-g-PAAm hydrogel. The calibration curve is illustrated below.

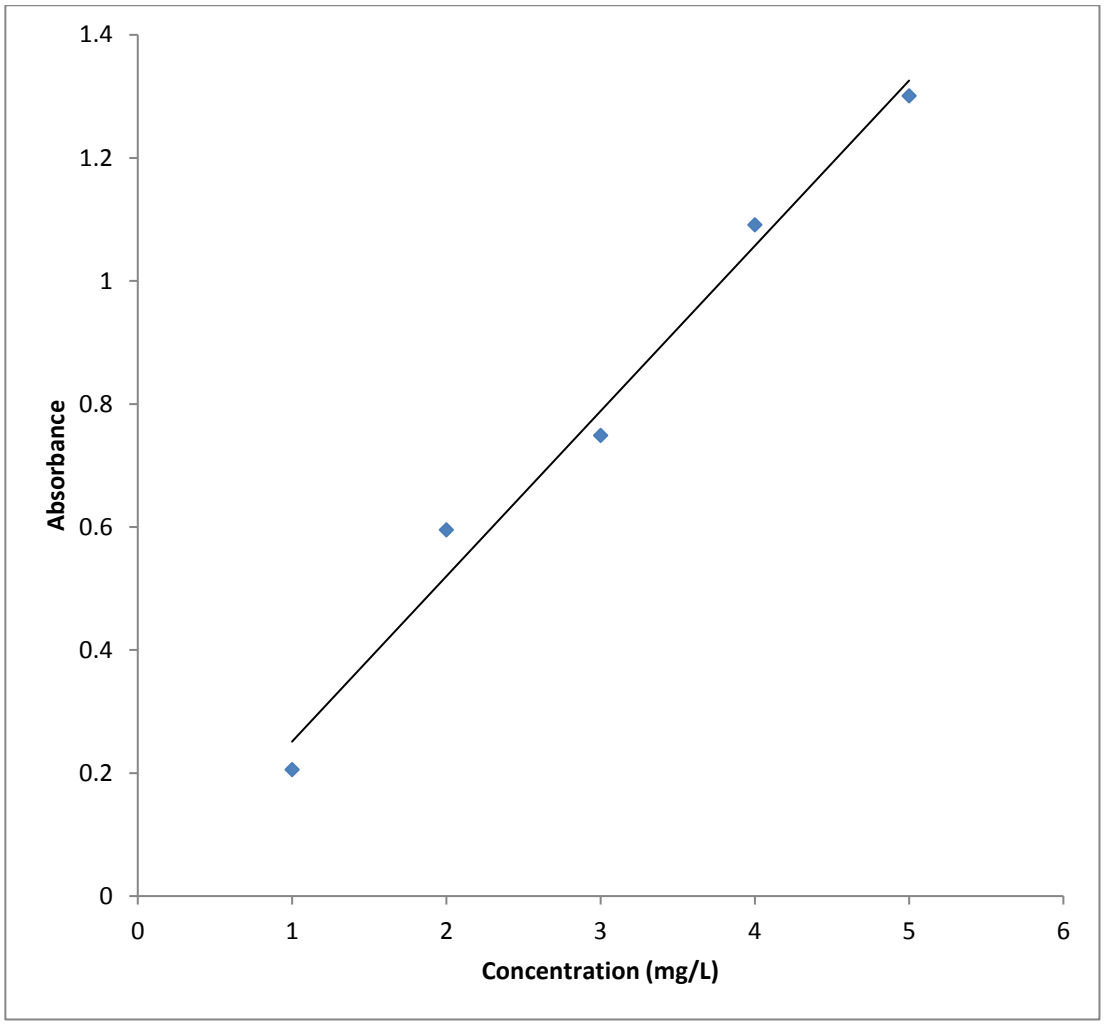

Figure 5: Calibration Curve of Methylene Blue for the Estimation of Dye Uptake by Adsorbent.

2.6.2 Batch Adsorption Experiment.

Batch adsorption experiments were performed at a temperature range of 25-50 ^{o}C using a set of 250 mL Erlenmeyer flask containing 0.025 g of adsorbent and 25 mL of

MB solution of different initial concentrations (10-100 mg/L). The MB solution was adjusted to varying pH range (2-12) using 1 M HCl and 1M NaOH solutions, this was then shaken at an agitation speed of 205 rpm for 1,440 min. After equilibrium is achieved, decantation and filtration were carried out and the equilibrium concentration of the dye was determined using a UV-visible spectrophotometer at maximum wavelength of 665nm. The percentage removal of MB dye and amount of dye adsorbed were calculated using the following equations.

$$\% \text{ Removal} = \frac{(C_0 - C_e)}{C_0} * 100 \quad (21)$$

$$q_e = \frac{(C_0 - C_e)}{M} V \quad (22)$$

where C_0 and C_e (mg/L) are the initial dye concentration and equilibrium dye concentration at a given time:

- q_e (mg/g) amount of MB dye in mg per gram of adsorbent.
- V (dm^3) volume of solution
- M (g) mass of hydrogel used

2.7 Swelling Studies of Hydrogel

Hydrogels (polyacrylamide and VCS-CT-g-PAAm with varying amounts of acrylamide) were immersed in buffered solutions of pH 2, 7 and 9 with temperature set at 25 ^oC was used to determine their swellability. The pH of the solutions was adjusted using 0.1 M HCl and 0.1 M NaOH. 0.05 g of hydrogel was placed in a beaker and filled with 50 mL of buffered solution and left for a specified time interval in other to attain equilibrium swelling. The excess water was blotted out using a filter paper before weighing. The swelling ratio was determined by the equation below,

$$Swelling\ \% = \left[\frac{(W_t - W_0)}{W_0}\right] * 100 \quad (23)$$

Where W_t is the weight of swollen hydrogel at a given time, and W_0 is the initial weight of the samples. The test was carried out in triplicate to obtain obtain a mean value.

2.8 Antibacterial Susceptibility Tests

2.8.1 Preparation of Blood Agar (BA)

10 g of blood agar base powder was dissolved in 238 mL of distilled water in a 500 mL conical flask and mixed thoroughly with frequent agitation and heating until it dissolved completely. The mixture was then autoclaved for 15 min at 121 ^{o}C and 776 mmHg. It was then allowed to cool down to 40 ^{o}C after which 12 mL of sterile blood was added and mixed thoroughly before pouring into sterile petri dishes.

2.8.2 Preparation of Muller Hinton Agar (MHA)

9.5 g of MHA powder was dissolved in 250 mL distilled water and mixed thoroughly with frequent agitation and heating until it dissolved completely. The mixture was autoclaved for 15 min at 121^{o}C and 776 mmHg. It was allowed to cool down to 50 ^{o}C before pouring into sterile petri dishes.

2.8.3 Preparation of Muller Hinton Broth (MHB)

This media is used for the determination of minimum inhibitory concentration (MIC) and minimum bactericidal concentration (MBC). 5.25 g of MHB dry powder is dissolved in 250 mL distilled water and mixed thoroughly with frequent agitation until completely dissolved. The mixture is autoclaved for 15 min at 121^{o}C and 776 mmHg. It was allowed to cool down then used for the antibacterial susceptibility test.

2.8.4 Antibacterial Susceptibility Test for CT-g-VTCS Film

E. faecalis, E. coli, Kleb spp., S. aureus and Methicillin-resistant S. aureus bacterial strains were selected as the target microbes to evaluate the antibacterial properties of the samples using the broth dilution and agar disk diffusion methods. The microdilution method was used as described previously by Aleanizy et al. (2018) with

some modification. The test microbes were grown for 20 h at 37 °C on Mueller–Hinton Agar (MHA; BD Diagnostic Systems, Sparks, MD, USA) except for MRSA strains, for which mannitol salt agar (MSA; BD Diagnostic Systems, Sparks, MD, USA) supplemented with 4% cefoxitin was used. The turbidity of the suspension was adjusted to 0.5 McFarland standard. Hundred microliters of the bacterial broth suspension was inoculated into 96-well microtiter plates, containing different concentrations of the samples (CT and CT-g-VTCS) serially diluted in cation-adjusted Mueller–Hinton broth (CAMHB, pH adjusted to 5.9). The obtained suspensions were incubated for 8 h at 37 °C. Then, 0.5 mL of the above solution was spread on an agar plate and cultured at 37 °C overnight. Control experiments without the samples (CT and CT-g-VTCS) were conducted in the same manner; and the bacterial growth was measured periodically. Count of viable colonies was read and multiplied by a dilution factor. Each experiment was performed in triplicate, and an average value was obtained. The minimum inhibitory concentration (MIC) was recorded as the lowest concentration of the samples where no visible growth was observed in the wells of the microtiter plates. The inhibition rate (AR%) was calculated using Eq. (24); the antibacterial activities of the CT and CT-g-VTCS were further tested through the agar disk diffusion method and the zone of inhibition was measured:

$$AR(\%) = \frac{a * x_0 - b * x_1}{a * x_0} \times 100 \tag{24}$$

where x_0 and x_1 are the number of colony-forming units (CFU/mL) in the absence of antibacterial agents and in the presence of antibacterial samples, respectively. The bacterial liquid dilution factors without and with antibacterial samples are represented by a and b, respectively.

2.8.5 Antibacterial Susceptibility Test for VCS-CT-g-PAAm Hydrogel

The target strains used in the antibacterial test were gram-positive *S. aureus* and gram negative *E. coli* bacteria. The spread plate method was used as described previously by Xin et al. (2016) with some modification. Freshly cultivated microbe were grown on Mueller Hinton Agar (MHA; BD Diagnostic Systems, Sparks, MD, USA), for 20h at 37^{o}C. Bacterial solution was prepared and the suspension turbidity adjusted to 0.5 McFarland standard. A further dilution was made to give a final concentration of $1*10^{6}$ CFU.

Pre-weighed amount of the hydrogels were put into 6-well plates containing 5 mL of bacterial suspension ($1*10^{6}$ CFU) , and kept for 2-24 h at 37 ^{o}C. At each time interval 10 uL of the bacterial suspension was removed from the well plates and serial dilution was carried out and a final 20 uL was then spread unto a blood agar plate, which were then incubated for 20 h at 37 ^{o}C and the grown colonies counted out. A test control was also performed without the hydrogel samples. The experiments were carried out in triplicate. The hydrogel killing percentage was calculated using the equation below.

$$Hydrogel\ killing\ (\%) = \left[\frac{(N_{control} - N_{sample})}{N_{control}}\right] * 100 \qquad (25)$$

($N_{control}$ and N_{sample} are the the number of colony forming units at the end of the incubation period on the blood agar plates of the control and hydrogel samples respectively.)

Chapter 3

RESULTS AND DISCUSSION

3.1 Grafting

The fabrication of CT-g-VTCS film with enhanced water solubility and improved antibacterial action was successfully synthesized through free radical graft polymerization as can be seen in the schematic pathway below (Figure 6). Path A gave a water soluble chitosan derivative and path B gave a crosslinked chitosan derivative.

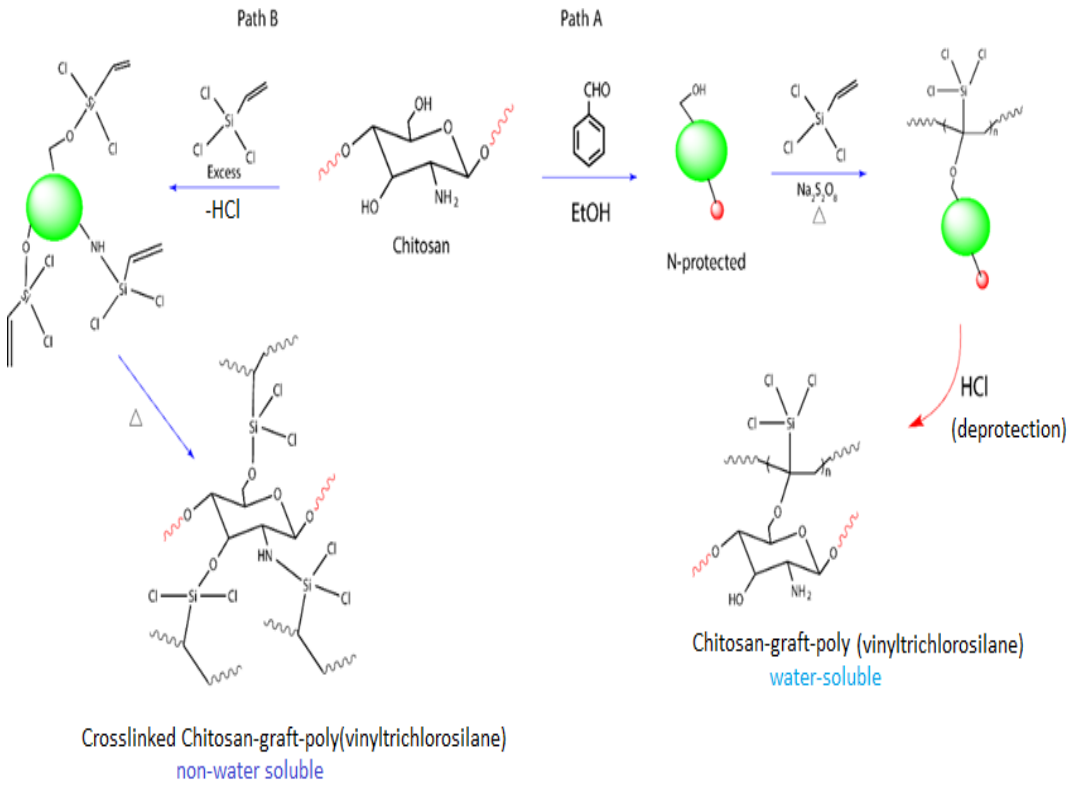

Figure 6: Schematic Pathways for the Synthesis of Chitosan-Graft-Poly (Trichlorovinylsilane) Derivatives.

The evidence of grafting can be seen from the physical characteristics of the products as while as spectrophotometric, imaging and constitutional characterization. The grafted products from CT-g-VTCS film and VCSCT-g-PAAm hydrogel can be seen in Figure7 and Figure8 respectively and the clear distinction from the initial starting materials can be observed from the images. The percentage grafting obtained was in the range of 48-80 %.

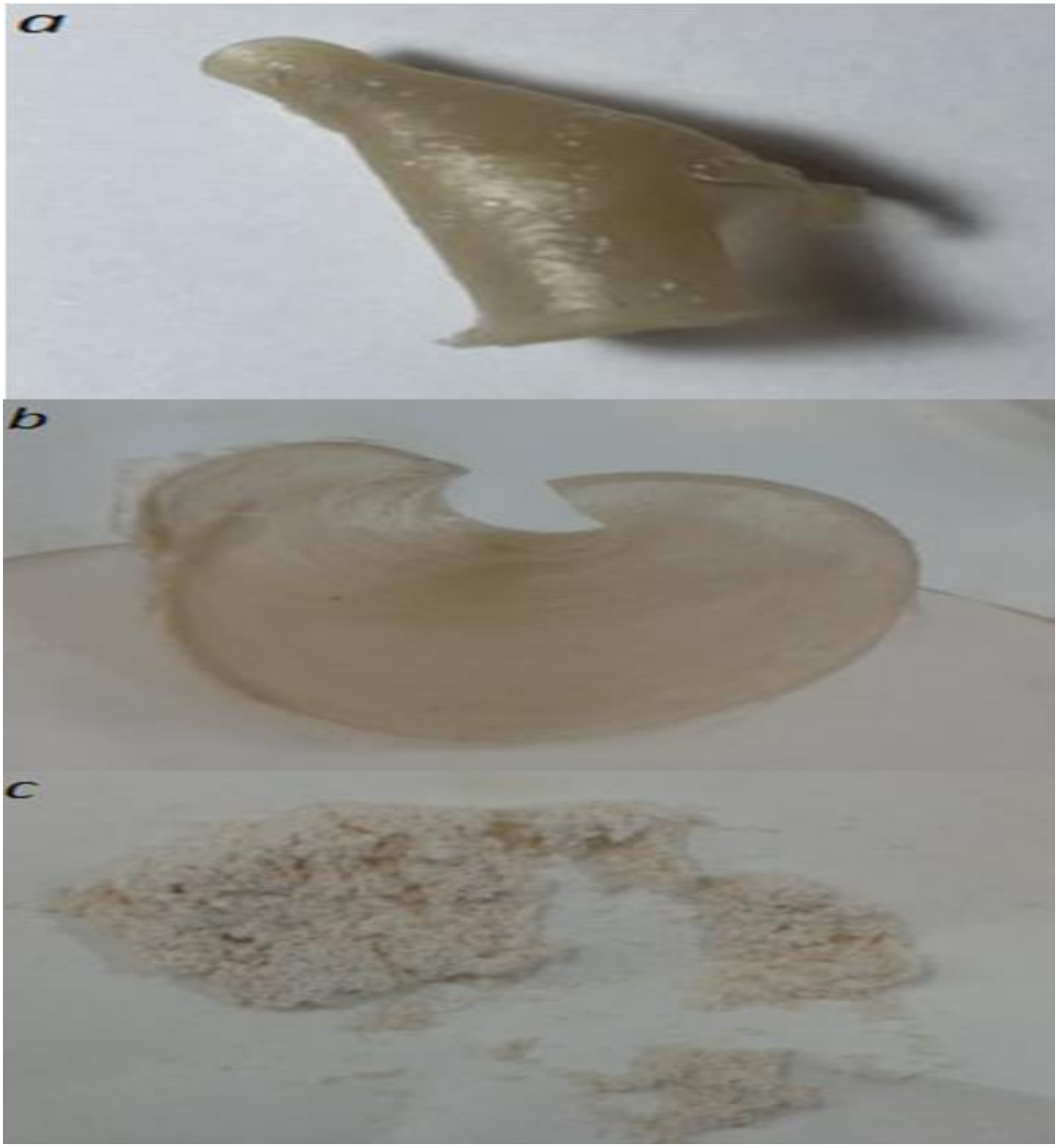

Figure 7: Images of (*a)* Outer View of Water Soluble CT-g-VTCS Grafted Film (*b*) Inner View of Water Soluble CT-g-VTCS Grafted Film (*c)* Water Insoluble CT-g-VTCS

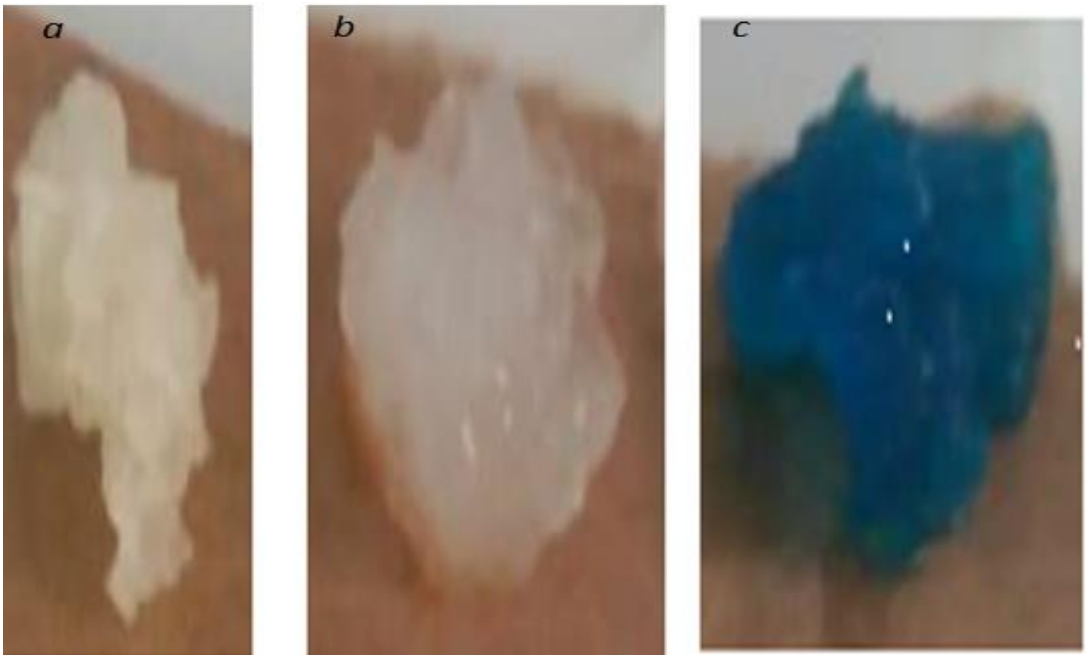

Figure 8: Images of (a) Dry VCS-CT-g-PAAm Hydrogel (b) Swollen/Wet VCS-CT-g-PAAm Hydrogel (c) MB Adsorbed VCS-CT-g-PAAm Hydrogel

3.1.1 Characterization of Grafted Vinyltrichlorosilane-Chitosan

3.1.1.1 Fourier Transform Infrared Spectrophotometry (FTIR)

The FTIR spectra of the samples are shown in Figure 8. The water insoluble product obtained via path B (Figure 6) was not characterized due to its lower antibacterial activity; hence, water-soluble CT-g-VTCS is discussed herein. The chitosan spectrum shows typical characteristic peaks of polysaccharide (Gritech et al. 2018; Yan et al. 2019; Chylin'sk et al. 2019; Amad et al. 2016; Ahmad et al. 2019; Algahtani et al. 2019, Kong et al. 2010). The strong band in the region of 3288–3489 corresponds to the N–H stretching and the intramolecular hydrogen bonds. The distinct peaks at 1642, 1356 and 1574 cm−1 confirmed the presence of residual N-acetyl groups (stretching of amide I: C=O), (stretching of amide III: C–N) and bending vibrations of amide II: N–H) (Oladipo 2015) as well as the symmetric C–H absorption band at 2921.3 cm^{-1}. Ahmad et al. (2016) and Ahmad et al. (2019) reported similar peaks for chitosan. In the case of VTCS-m-CT, the amide I–III bands are obviously less affected except the

slight reduction in the band at 1727.2 cm^{-1}. Notably, the band at 969.4 cm^{-1} in the VTCS-m-CT is attributed to Si–O–C–O= group which might be indicative of interaction of O–H bending in the chitosan and the Si–Cl of the TVS (Sluszny et al 2001). Also, the obvious characteristic peaks at 572.7 and 698.2 cm^{-1} are indicative of Si–Cl (bend) and 3064–3020 cm^{-1}, indicating the availability of the Si–CH=CH2 group (Sluszny et al 20012; Komata et al. 2016).

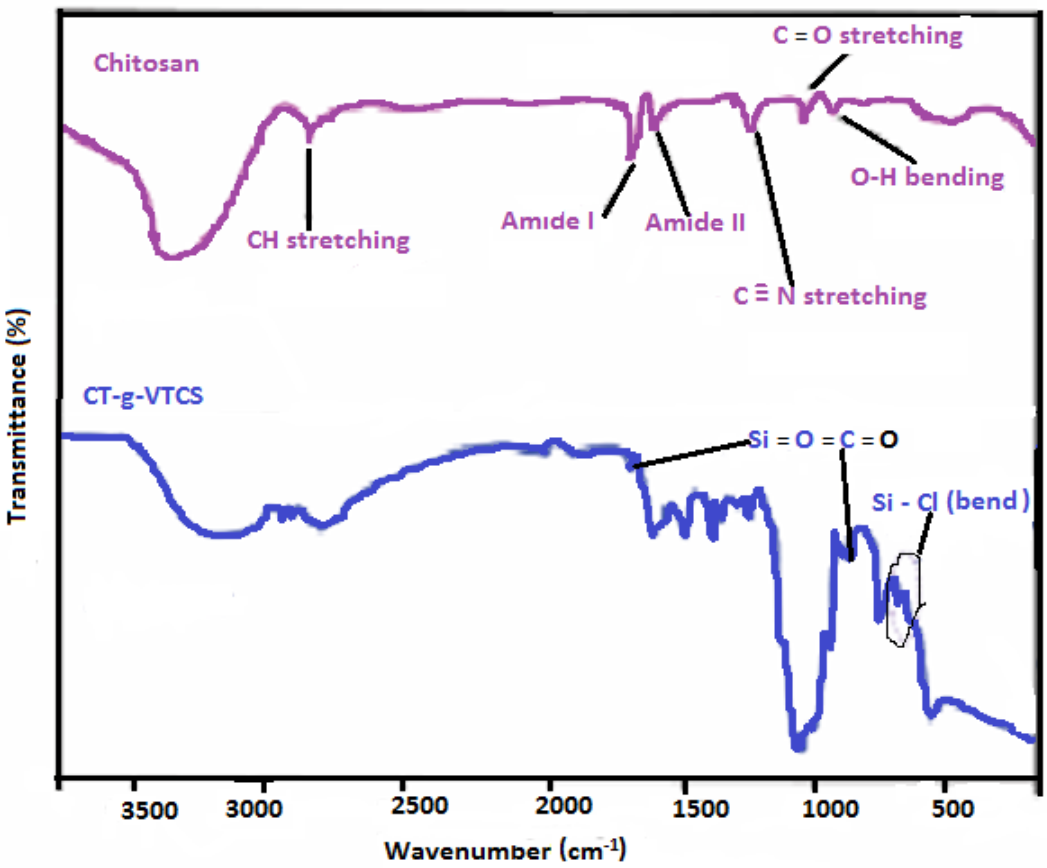

Figure 9: (a) FTIR Spectra of Chitosan and Prepared CT-g-VTCS Film

3.1.1.2 X-ray Diffraction (XRD)

XRD patterns of the samples are shown in Figure 10. The distinct chitosan peaks are observed at 2θ=10.4° and 2θ=19.8° (Yusof 2019) which demonstrate the existence of crystallinity in the CT sample. Although the intensities of these peaks decreased in the XRD pattern of CT-g-VTCS. The interaction of VTCS with chitosan results in the

appearance of peaks at 2θ values 28.1° (111) and 47.3° (220), which correspond to silicon peaks and are consistent with the reflections indexed in standard X-ray diffraction powder patterns (JCPDS 77-0010). The sharpness of these peaks reflect the crystalline nature of the CT-g-VTCS, and the XRD results are consistent with the observed functional groups in the FTIR. The nitrogen adsorption isotherms results indicated that the CT-g-VTCS exhibits type-IV isotherms according to the IUPAC (Oladipo et al. 2015); its BET specifc surface area (288 m^2 /g) is significantly higher than that of CT (145 m2 /g). Also, the CT-g-VTCS pore size (2.95 nm) denotes the presence of mesopores and it is larger than that of CT (2.15 nm).

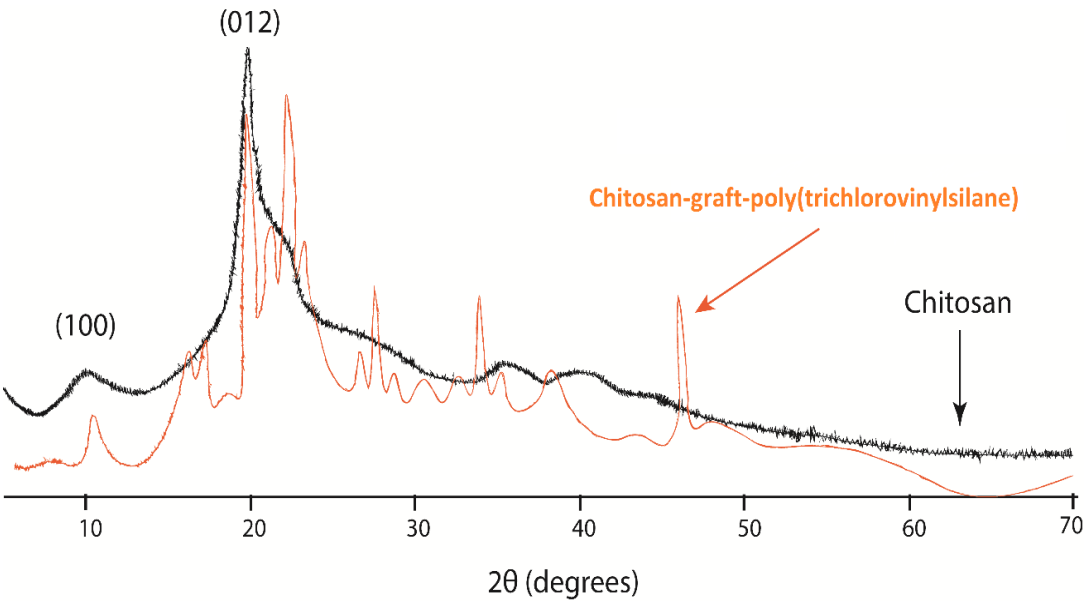

Figure 10: XRD Pattern of Chitosan and Prepared CT-g-VTCS Film

3.1.1.3 SEM and EDX

The SEM and EDX of CT and CT-g-VTCS are represented in Figure 11. CT has a smooth surface when compared with CT-g-VTCS which has a lump-like structures on the surface. This dense rough surface of CT-g-VTSC is consistent with a two phase morphology in graft and block copolymers. This morphology exhibited by CT-g-VTCS supports the grafting of VTCS onto chitosan backbone. The increased

roughness of CT-g-VTCS likely contributed to its higher solubility in water as molecules of water are able to navigate easily through the pores of the membrane. Figure 11c shows that the EDX spectrum of CT contains elemental C, N and O, and the N is attributed to the amine ($–NH_2$) group of chitosan. The presence of elemental Si and Cl is related to the VTCS in the EDX spectrum of the CT-g-VTCS. Also, grafting of VTCS onto the CT led to a lower O content; notably, the C/O ratio in CT is lower than that in CT-g-VTCS. This is attributed to the interaction of the C-6-OH of the CT with the Si–Cl of the VTCS which is consistent with the FTIR and XRD results.

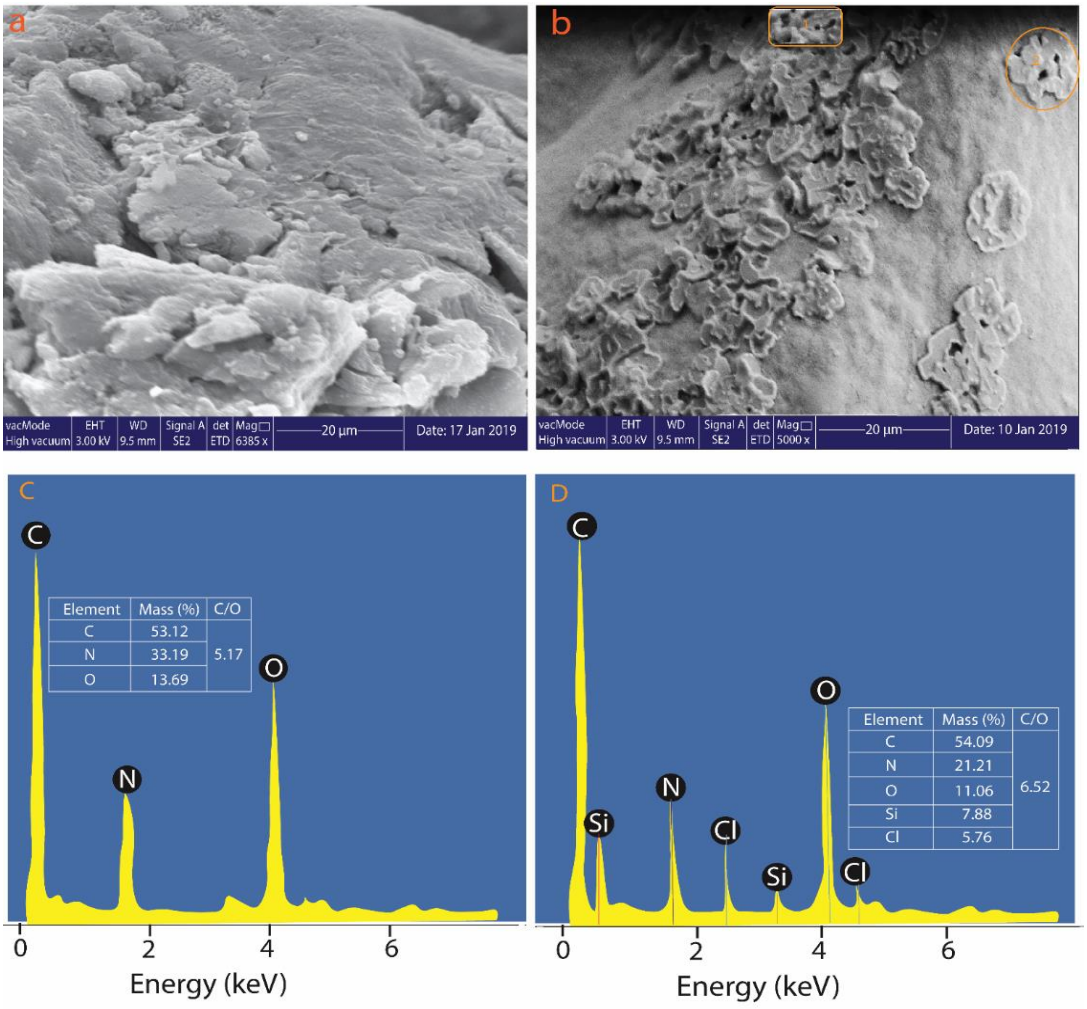

Figure11: (a-b) SEM Images (c-d) EDX Spectra of Chitosan and CT-g-VTCS Respectively

3.2 Water Solubility of CT-g-VTCS and CT

The focus of this research is not only to improve the antibacterial activity of chitosan but also to enhance its water solubility. Therefore, the water solubility of CT, cross-linked chitosang-g-poly(trichorovinylsilane) (CT-g-VTCSB) and CT-g-VTCS was compared (Table X). The results show that the transmittance percentage of CT-g-VTCSB, CT-g-VTCS and CT was 78, 99.6 and 55.8% in distilled water respectively. Note that the solubility of CT in acetic acid is ~2.5 times higher than that of CT-g-VTCS in acetic acid indicating that the CT-g-VTCS (18.1 mg/mL) had better solubility at neutral pH condition than CT (5.5 mg/mL) and CT-g-VTCSB. The improved water solubility of CT-g-VTCS is caused by the introduction of VTCS groups on the CT backbone and intensely enhanced crystalline structures of CT-g-VTCS. Hence, CT-g-VTCS can be directly applied in solutions like ointment used in medical fields.

Table 1: Water solubility and % Transmittance (in H_2O) of CT, CT-g-VTCS and CT-g-VTCSB

Polymer	Water mg/mL	% Transmittance in water
CT	5.5	55.8
CT-g-VTCS	18.1	99.6
CT-g-VTCSB	6.2	78

3.3 Antibacterial Properties of CT-g-VTCS

To determine the efficacy of the synthesized CT-g-VTCS film against viable strains of bacteria, the minimum inhibitory concentration (MIC) was evaluated. This is the minimum concentration of the product that is needed to inhibit the growth of bacteria colonies. The minimum bactericidal concentration (MBC) was also determined. This is the minimum amount of product that is required to kill viable bacteria colonies.

3.3.1 Minimum Inhibitory Concentration and Minimum Bactericidal Concentration

The MICs of the CT-g-VTCS and CT in water and acetic acid were determined to evaluate their antibacterial activities using the 96 micro well plate (Fig 12). Results in Figure 13a and Table Z evidently indicated that CT-g-VTCS in water had lower MIC values for *S. aureus* and *E. coli* than CT in acetic acid. The MICs of CT-g-VTCS in the water against *Kleb spp*., *E. faecalis* and *MRSA* were slightly lower than that of CT in acetic acid. Under the same conditions (in acetic acid), the MICs values showed that the antimicrobial activity of CT-g-VTCS is analogous to CT against *S. aureus* and *E. faecalis.* (0.156 mg/mL); however, the CT-g-VTCS exhibited less antibacterial activity against *E. coli, Kleb spp.* and *MRSA* (0.313 mg/mL). This phenomenon might be associated with the functional groups on the samples and the surface charge of the bacteria strain (Li et al. 2019). In an acetic medium, the *S. aureus* carried more negative charges than E. coli due to its lower isoelectric point; hence, the antibacterial activities of CT and CT-g-VTCS were dominated by the interaction between the more negatively charged *S. aureus* and the positively charged CT and CT-g-VTCS groups. These results are in agreement with other reports where the chitosan and its derivatives exhibited lesser antibacterial activity against gram-negative bacteria than gram-positive bacteria strains (Bakshi et al. 2018; Chen et al. 2016; Yusof et al. 2019; Tabriz et al. 2019; Li et al 2019). In contrast, the CT-g-VTCS activity is pronounced against *S. aureus* (0.039 mg/ mL) and *E. coli* (0.078 mg/mL) in water than in acetic acid (0.156–0.313 mg/mL). This may be attributed to the fact that the CT-g-VTCS was more soluble in water and, thus, could easily interact with the bacteria. The MIC results of the antibacterial property of CT-g-VTCS against each bacterium defer based on their cell wall structure. MBC, the lowest concentration of the as-synthesized

antibacterial agents that kills ≥99.9% of the initial bacterial inoculum was investigated as described elsewhere (Abureesh et al. 2018; El-Shahaw et al. 2018 30). The MBC values of the CT-g-VTCS in water (3.12–12.5 mg/mL) were comparable to that in acetic acid (3.33–18.5 mg/mL), whereas CT shows higher MBC values (20.2–61.3 mg/mL) in the 24-h treatment process. The strong electron withdrawing group (–Cl–) on the CT-g-VTCS strengthens the positive charge density of CT-g-VTCS and subsequently reduces the charge density on the bacterial surface causing a decrease in cell viability and death of the bacteria after 24 h. Furthermore, the time-kill test of CT-g-VTCS against *S. aureus* and *E. coli was* studied.

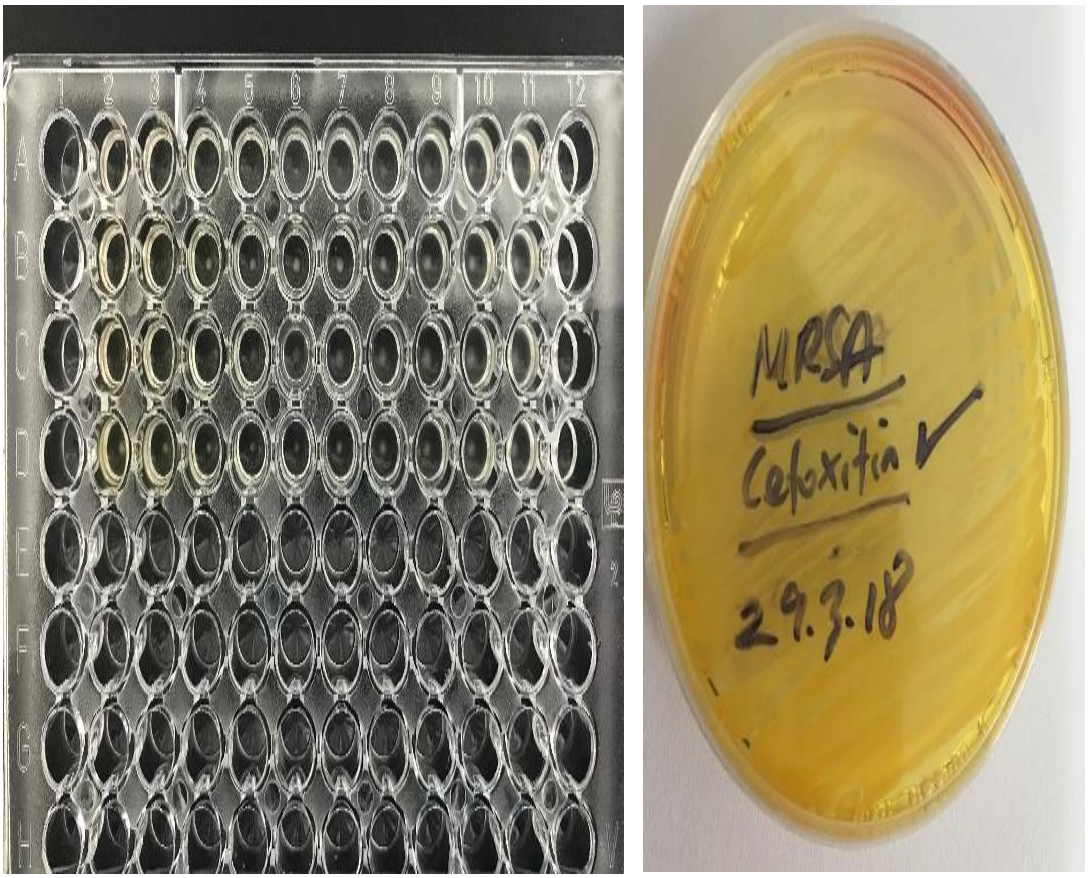

Figure 12: Applications of Broth Microdilution Method (Left) and Yellowish Growth of MRSA Strain on 4% Cefoxitin Supplemented MSA.

Table 2: MIC Values of CT and CT-g-VTCS in Acetic Acid and Water

Bacteria	MIC of CT in acetic acid	MIC of CT-g-VTCS in acetic acid	MIC of CT-g-VTCS in water
E. coli	0.156 mg/mL	0.313 mg/mL	0.078 mg/mL
S. aureus	0.156 mg/mL	0.156 mg/mL	0.039 mg/mL
E. faecalis	0.156 mg/mL	0.156 mg/mL	0.156 mg/mL
***Klebsiella* spp.**	0.156 mg/mL	0.313 mg/mL	0.156 mg/mL
MRSA	0.156 mg/mL	0.313 mg/mL	0.156 mg/mL

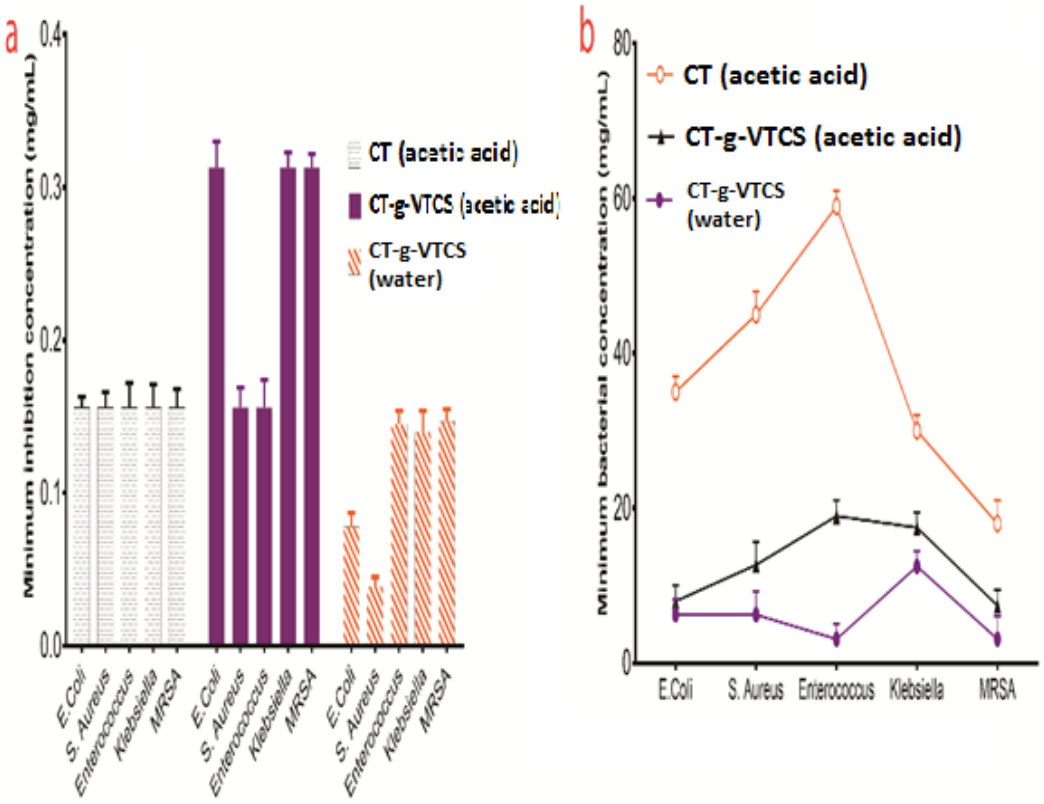

Figure 13: (a) Minimum Inhibitory Concentration (MIC) (b) Minimum Bactericidal Concentration (MBC) of CT-g-VTCS and CT Against 5 Bacterial Strains in Acetic Acid and in Water.

3.3.2 Time-Kill Curve Study

The method for the kill study was reported previously (Blondeau et al. 2015). As indicated in Figure 13a-b, the control experiments showed that the bacterial species entered the rapid growth logarithmic phase after 2 h of adjusted phase and then entered the stable growth phase after 5 h. Meanwhile, the incubation of the bacterial broths with various concentrations of CT-g-VTCS significantly reduced bacterial growth during 24 h test. Evidently, obtained results supported the bacteriostatic effect of CT-g-VTCS, notably in the logarithmic growth phase. Specifically, exposure of 10^7 CFU/mL S. aureus to 0.325 mg/mL of CT-g-VTCS gave a 6.69 log10 reduction (~72% kill) in viable cells after 4 h which increased to 8 log10 reductions (>82% kill) by 24. When the CT-g-VTCS concentration was increased to 5 mg/mL, it gave 5.04

(*E. coli*) and to 6.18 (*S. aureus*) log10 reduction by 24 h (88–93% kill) after 6 h. Following 24 h of 5 mg/ mL CT-g-VTCS exposure, a ~0.08 log10 reduction (>99.9% kill) was seen for both bacteria species.

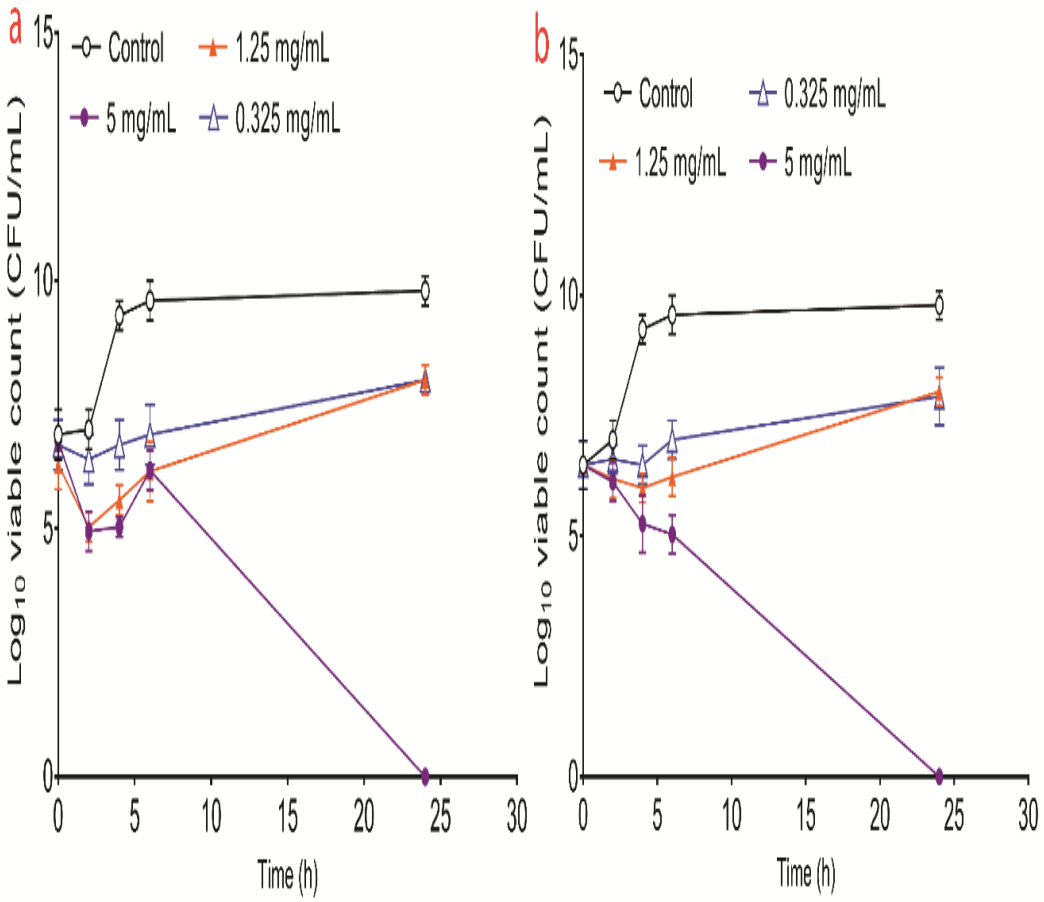

Figure 14: Time-kill Curve Analyses of the Antibacterial Activity of CT-g-VTCS Against (a) *S. aureus* (b) *E. coli* in Comparison to Control Experiments

3.3.3 Zone of Inhibition

The results of antibacterial activities of CT and CT-g-VTCS using the agar disk diffusion method are shown in Figure 15. The CT-g-VTCS produced inhibition zones of 23 and 10.9 mm when exposed to 10^7 and 10^9 CFU/mL S. aureus, respectively. In contrast, 20 mg/mL of CT revealed that the inhibition zone of the chitosan against S. aureus was smaller than that of the CT-g-VTCS. This further confirmed the

introduction of VTCS onto the chitosan backbone not only improved its water solubility but also enhanced its antimicrobial activity. The presented results are in agreement with other reports on the antibacterial activity of chitosan derivatives against commonly studied bacteria strains (Gazi et al. 2012; Aleanizy et al. 2018; Oladipo et al. 2015; Yusof et al. 2019; Tabriz et al. 2019; Li et al. 2019; Abureesh et al. 2018; El-Shahawy et al. 2018; Blondeau et al. 2015; Pan et al. 2019; Cao et al. 2019; Bharathi et al. 2019; Merlusca et al. 2018; Yu et al. 2018). Table 3 shows the MIC, MBC and inhibition zone diameters of chitosan and its derivatives against *S. aureus* and *E. coli*. The CT-g-VTCS evidently demonstrated comparatively high inhibitory effects on the investigated microorganisms; even though the exact mechanisms by which CT-g-VTCS disrupts the bacterial cells remain unclear, its improved antibacterial properties and water solubility make it a good candidate for use in micro-gel cream, ointments and wound dressings. Considering the overall results, the VTCS grafted chitosan prepared in this study exhibited improved antibacterial and water solubility properties.

Table 3: MICs, MBCs and Inhibition Zones of CT-g-VTCS and Reported Chitosan derivatives

Sample			Escherichia coli				Staphylococcus aureus			Ref.
	Dosage	Solubility	MIC	MBC	Z		MIC	MBC	Z	
CT	20	Acetic acid	156	35.0	-		156	45.0	5.4	This study
CT-g-VTCS	20	Acetic acid	313	8.0	-		156	12.7	-	This study
CT-g-VTCS	20	Water	78	6.25	-		39	6.25	23	This study
CT nanoparticle	75	Acetic acid	30	50	-		15	35	-	(Pan 2019)
CT–MoS_2	10	Acetic acid	2	-	-		16	-	-	[Cao 2019]
LMW.DIC.CNPs	75	Acetic acid	-	-	-		35 ± 2	-	18 ± 0.5	[Alqahtani 2019]
CT–ZnO	40	Acetic acid	-	-	25.5		-	-	22.5	[Bharathi 2019]
CTS–GA	-	Acetic acid	200	11.36	-		400	-	12.65	[Li 2019]
Cobalt ferrite–CT	1000	Acetic acid	-	-	-		125	62.5	39.5	[ElShahawy 2019]
CT/ZnO-PVP	30	Acetic acid	-	-	23.0		-	-	24	[Karpuraranjith 2107]
N-Q3CS	10000	Water	-	-	15.0		-	-	14.5	[Chen 2016]
Q3B3CS	10000	Water	-	-	18.1		-	-	18.0	[Chen 2016]
Ciprofloxacin	20	Water	0.0002	-	-		0.0009	-	-	Control

CT: Chitosan
CT-MoS_2: Chitosan – molybdenum disulfide nanocomposite
LMW.DIC.CNPs: Low molecular weight diclofenac sodium-loaded chitosan nanoparticles
CTS–GA: Gallic acid-grafted chitosan
CS/ZnO-PVP: Chitosan/zinc oxide-polyvinylpyrrolidone
N-Q3CS: N–quaternary chitosan
Q3B3CS: N–quaternary ammonium-O-sulfobetaine-chitosan
Z: Inhibition zone (mm), MIC, MBC and dosage are in µg/mL.
–: Not reported
Average values of at least three experiments with a standard deviation of ≤3% are presented.
A commercial drug (Ciprofloxacin) was used for the control test.

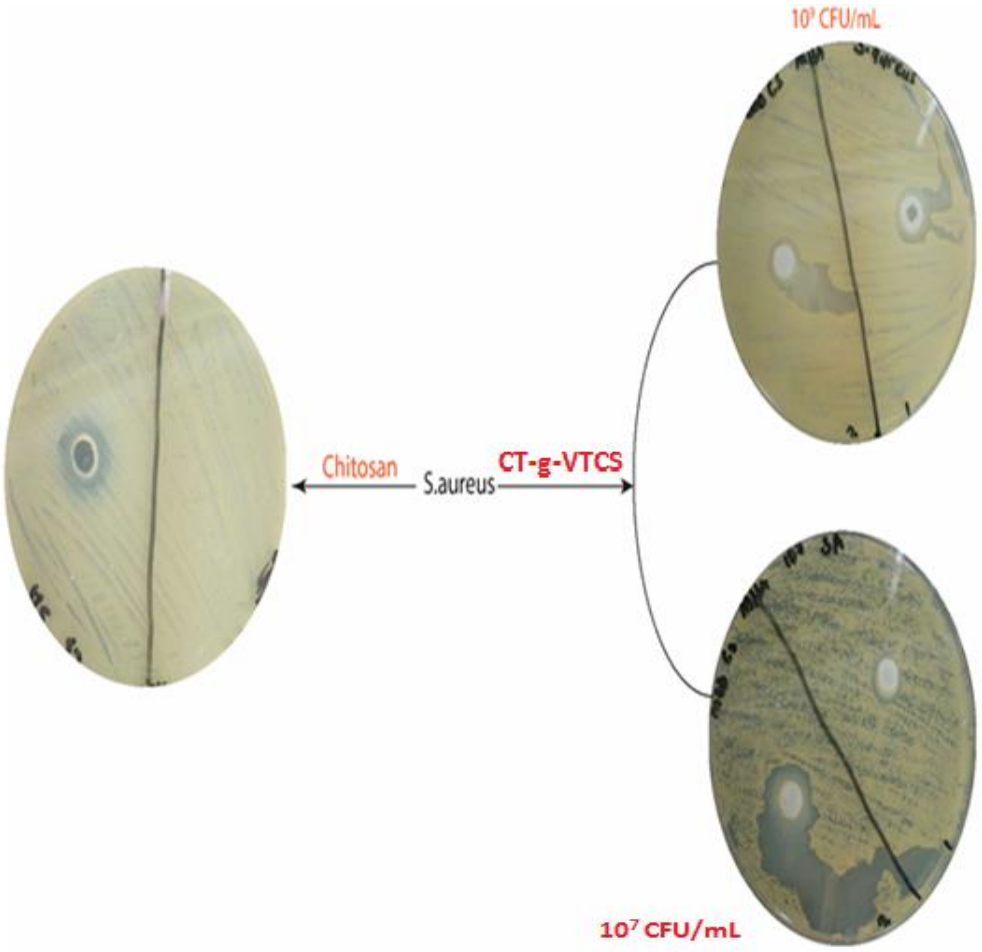

Figure 15: Digital Images of *S. aureus* Colonies after Treatment with 20 mg/mL of CT and CT-g-VTCS for 24 h Showing the Zone of Inhibition.

3.4 Characterization of VCSCT-g-PAAm hydrogel

The synthesis of chitosan-poly(vinyldichlorosilane) graft polyacrylamide is illustrated by the scheme below (Figure 16). An inter penetrating network (IPN) of PAAm and VCS-CT is formed in the presence of APS and MBA as the crosslinker.

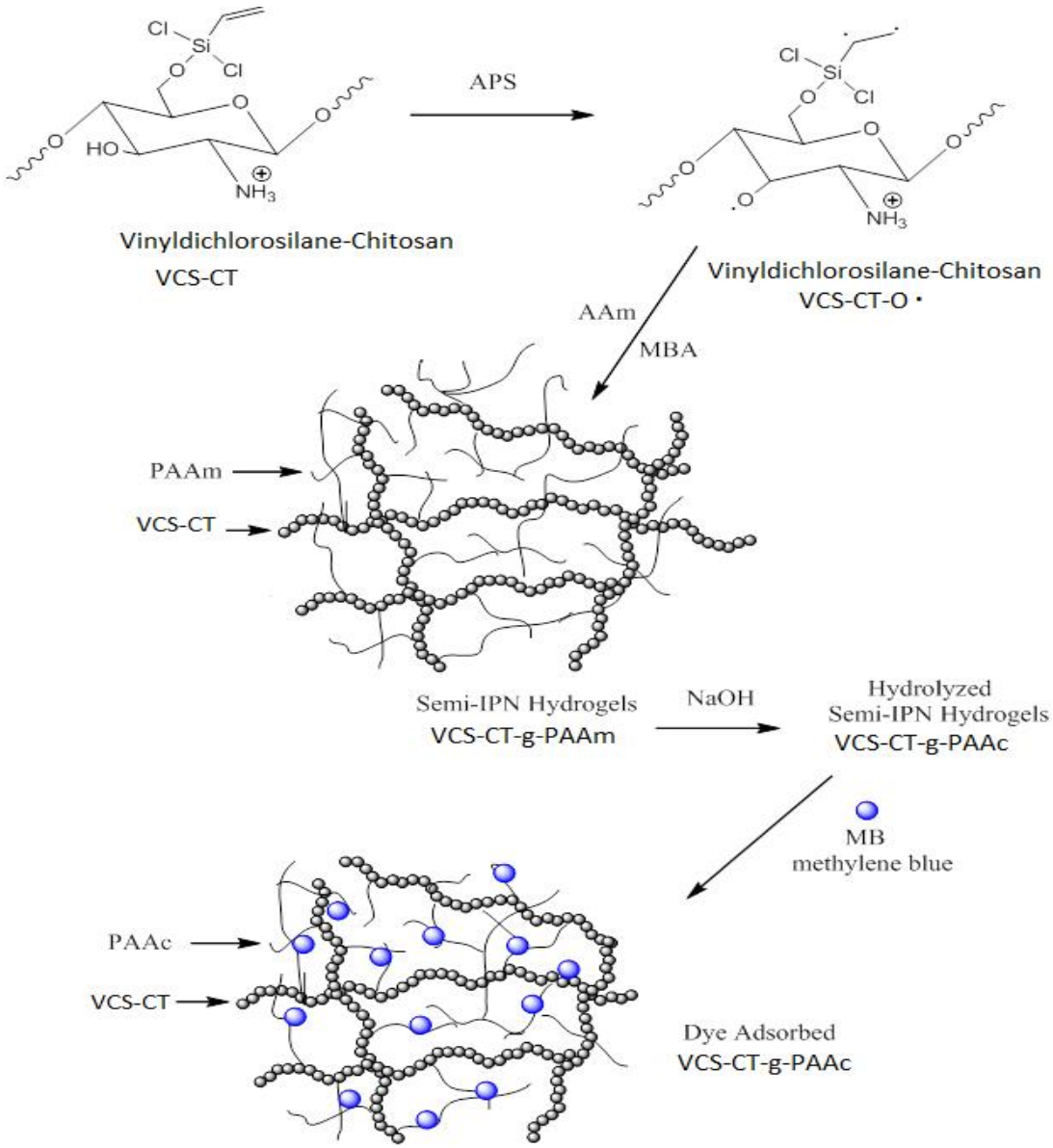

Figure 16: Schematic Pathways for the Synthesis of Chitosan-vinyltrichlorosilane–graft- Polyacrylamide Hydrogel Derivative**.**

3.4.1 FTIR Characterization of VCSCT-g-PAAm Hydrogel

The FT-IR spectra of the hydrogels are shown in Figure17. From the FTIR spectra of VCSCT-g-PAAm hydrogel (Figure17b) and polyacrylamide hydrogel (Figure17a), there is a marked difference in the frequencies band. The characteristic peaks at 561.92 and 766.6cm^{-1} on VCSCT-g-PAAm are indicative of Si-Cl (bend). The strong bands in the region of 3288-3489cm^{-1} in both spectra corresponds to the, N-H stretching and the intramolecular hydrogen bonds. The distinct peaks at 1654 and 1608 cm^{-1} on both

spectra confirmed the presence of residual N-acetyl groups(stretching of amide I:C=O) and (bending vibration of amide II:N-H); as while as the symmetric C-H absorption band at 2929cm^{-1}

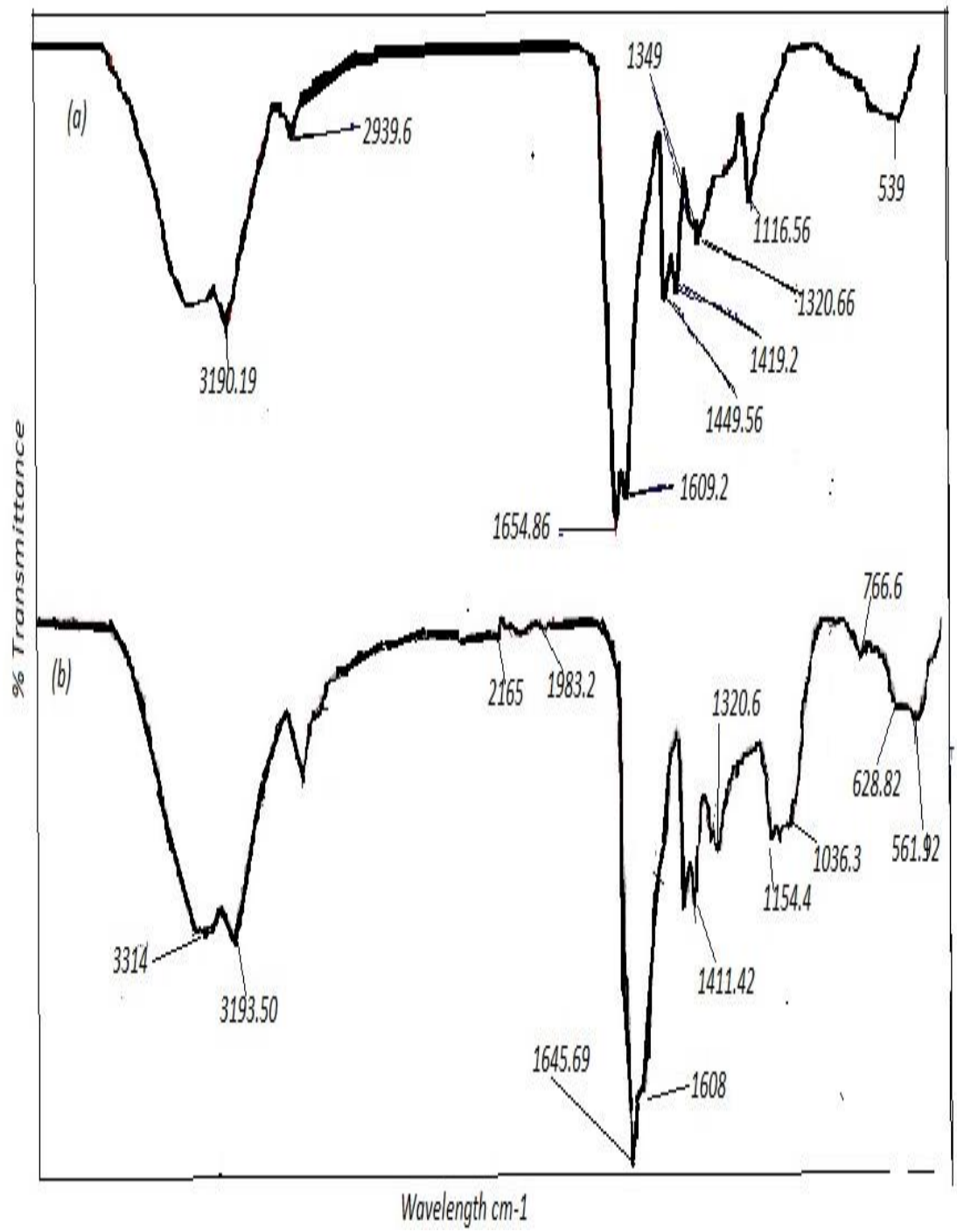

Figure 17: FTIR Spectra of (a) Polyacrylamide Hydrogel (b) VCSCT-g-PAAm Hydrogel

3.4.2 Effect of Gelation Time

Figure 18 shows the hydrogels with different molar ratios of PAAm and VTCS-m-CT all formed within 15mins. As the amount of acrylamide decreases the gelation time incresaes, which can be attributed to reduction in the available site of reaction on the acrylamide chain.

Figure 18: Hydrogel Formation with Different Ratios of Vinyltrichlorosilane Chitosan/Acrylamide Combination. Molar Ratio of Acrylamide Increases from Left to Right 0:1, 1:3, 1:5, 1:7 and 1:9.

3.5 Dye Adsorption Parameters

3.5.1 Effect of Adsorbent Dosage

The adsorption efficiency of adsorbent dosage was studied using 0.025-0.075 g and 25 mL of 10 mg/L adsorbate at 25 ^{o}C and pH 12. As can be seen in Figure19 the adsorption efficiency of the adsorbent slightly increases with increase in dosage. This can be attributed to the increased number of available active sites for adsorption on the adsorbent (Anwar et. al 2010), although no significant increment was noticed after 0.075 g.

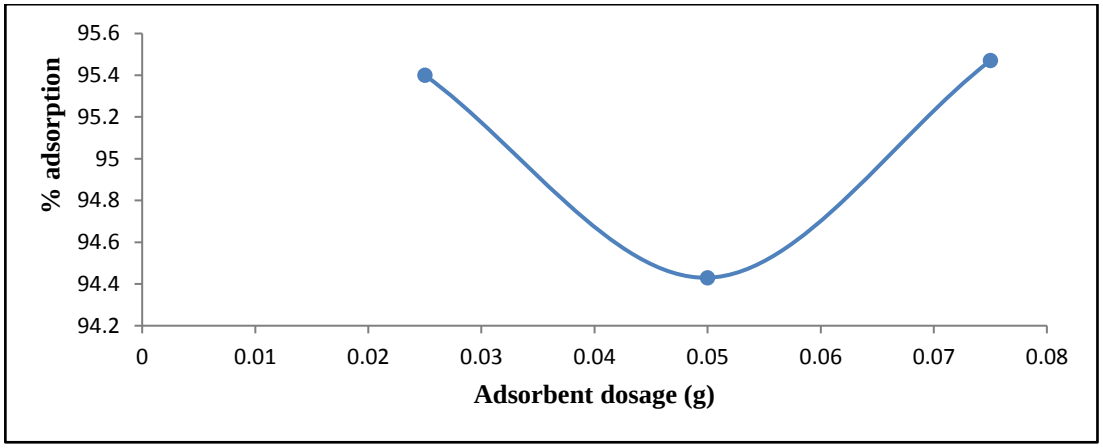

Figure 19: Effect of Dosage on the Adsorption of MB Onto VCS-CT-G-Paam Hydrogel

3.5.2 Effect of Concentration of Dye

The effect of initial MB concentration on the amount of dye adsorption and percentage removal of dye was studied and can be seen in Figure20. Different concentrations of MB were prepared ranging from 10-100 mg/L and the experiment was carried out at 25 ^{o}C, pH 12 and for 24 h. As the concentration of MB increases there is an enhanced increase of the uptake of MB dye onto VCS-CT-g-PAAm hydrogel (Figure18b). This can be attributed to increased collisions between the dye molecules as a result of bulk density of the dye molecules thereby prevailing over any liquid to solid phase barrier. Nevertheless, there was a gradual decrease in the percentage removal of dye (Figure18a), with complete adsorption been achieved at lower concentration. With the increase in MB concentration , the adsorbent active sites bind to the dye molecules and gets to a point of saturation where no dye molecules can be adsorbed(Olgun and Atar 2012).

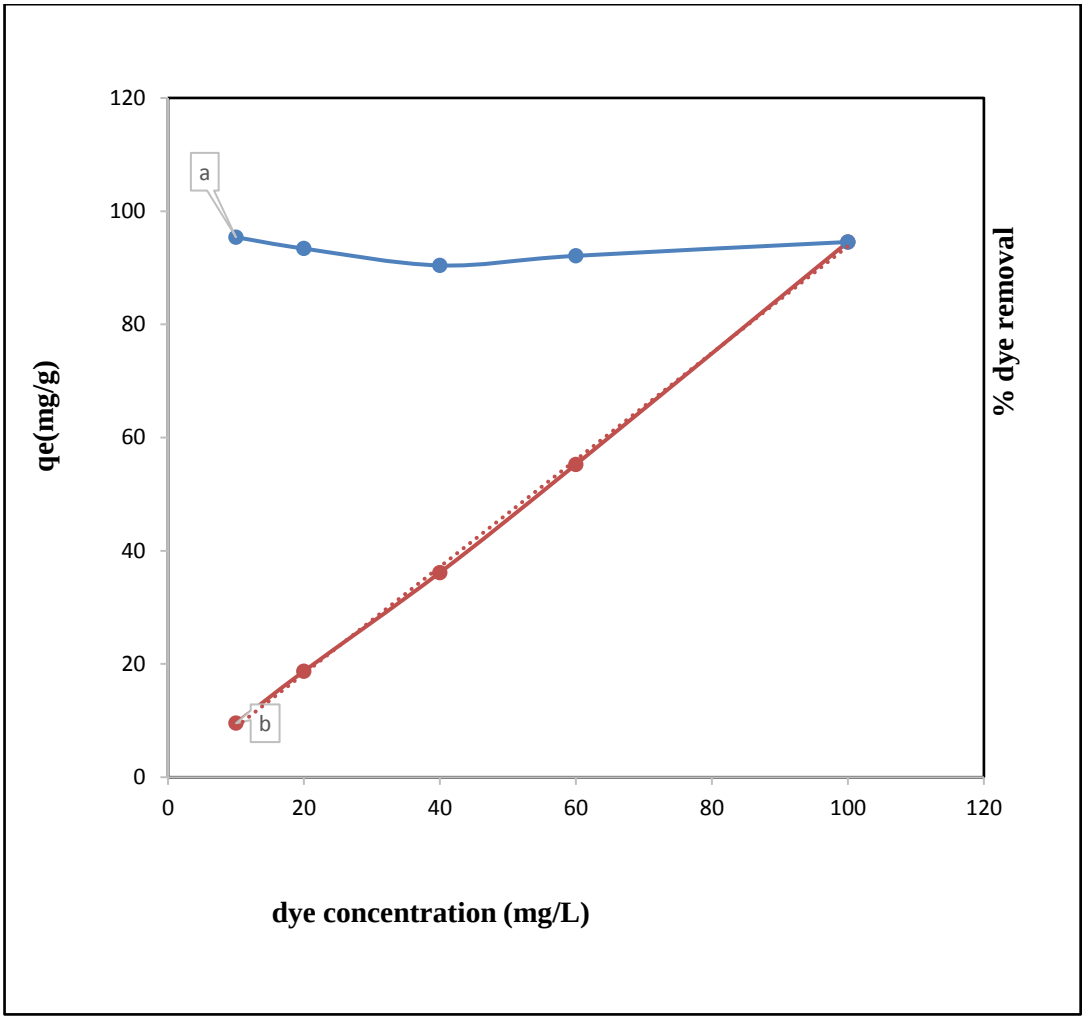

Figure 20: Effect of Initial Dye Concentration on the Adsorption of MB onto VCS-CT-g-PAAm Hydrogel

3.5.3 Effect of pH of Dye Solution

The effect of pH of the dye solution was studied and varied between 2-12. From the results obtained the adsorption of MB increases as the pH increases as can be seen from Figure21. The maximum adsorption occurred at pH 12, this is consistent with the adsorption of acrylamide based hydrogel at higher pH as reported by other researchers.Protonation of functional groups such as carboxyl and alcoholic groups occurs at pH <3, this decreases the adsorption efficieny while deprotonation of these functional groups occurs at pH > 8 and increases the adsorption efficiency (Al-qudah et. al 2014).

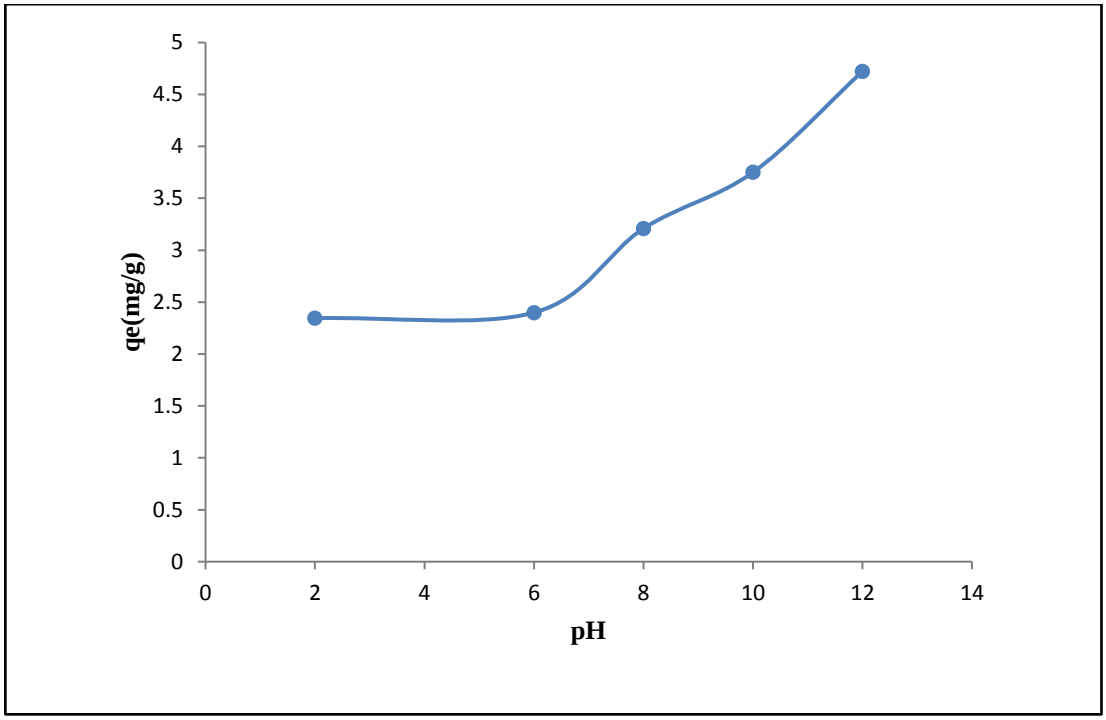

Figure 21: Effect of pH on the Adsorption of MB onto VCS-CT-g-PAAm Hydrogel

3.5.4 Effect of Temperature

Temperature effect studies for the adsorption of MB onto VCS-CT-g-PAAm was performed at 25, 35 and 50 ^{o}C for 24 h using 25 mL of 20 mg/L adsorbate solution and 0.05 g of adsorbate at pH 12. There was a minimal increase in the adsorption of MB as the temperature was increased signifying an endothermic process. The adsorption capacity of MB increased from 9.753-9.777 mg/g onto the VCS-CT-g-PAAm hydrogel at 25-50^{o}C as seen from Figure 22. This can be ascribed to the increase in the kinetic energy of the MB molecules giving them adequate energy to prevail over the bulk layer and be adsorbed onto the crevice of the hydrogel network (Chen et. al 2011).

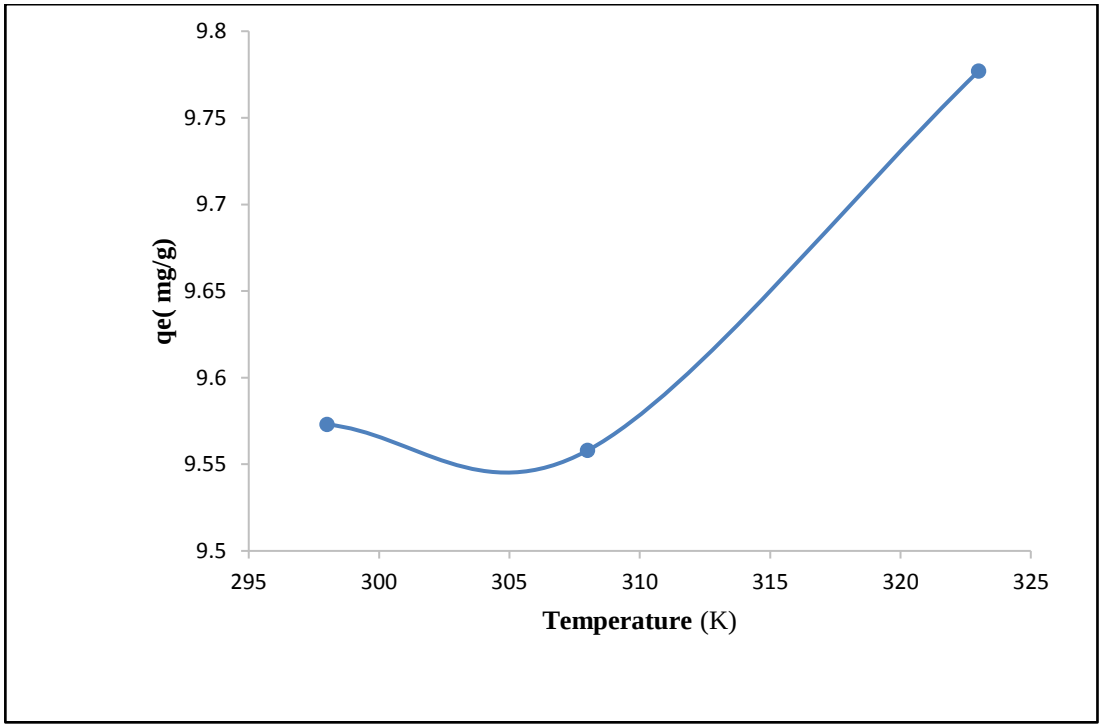

Figure 22: Effect of Temperature on the Adsorption of MB onto VCS-CT-g-PAAm Hydrogel.

3.6 Adsorption Isotherms

To fully understand the adsorption behaviour of the the prepared VCS-CT-g-PAAm hydrogel, four adsoprtion isotherm models (Langmuir, Freudlich, Redlich-Peterson and Sips) were used. The linearized forms of their equations are given in equations 4, 6, 9 and 11 respectively. The calculated values of each isotherm are presented in Table 4. Fig 23, 24, 25 and 26 illustrates the different isotherms of Langmuir, Freundlich, Redlich-Peterson and Sips respectively. The obtained experimental data fitted well into the four models, however the correlation coefficient for Langmuir (R^2) 0.986 was observed to best fits the data obtained as compared to other models. The R_L values (Figure25) obtained from Langmuir isotherm ranged from 0.703-0.283, indicating that the monolayer adsorption of MB onto VCS-CT-g-PAAm hydrogel was favourable.

Table 4: Adsorption Isotherm Parameters for Adsorption of MB onto VCS-CT-g-PAAm hydrogel.

	R^2	K_L (L/mg)	n	R_L	K_F (mg/g)	q_m (mg/g)
Langmuir model	0.986	0.042	-	0.703-0.283	-	93.45
Freundlich model	0.978	-	1.42	-	1.21	
Redlich-Peterson model	0.888	-	-	-	-	
Sips	0.987	-	-	-	-	

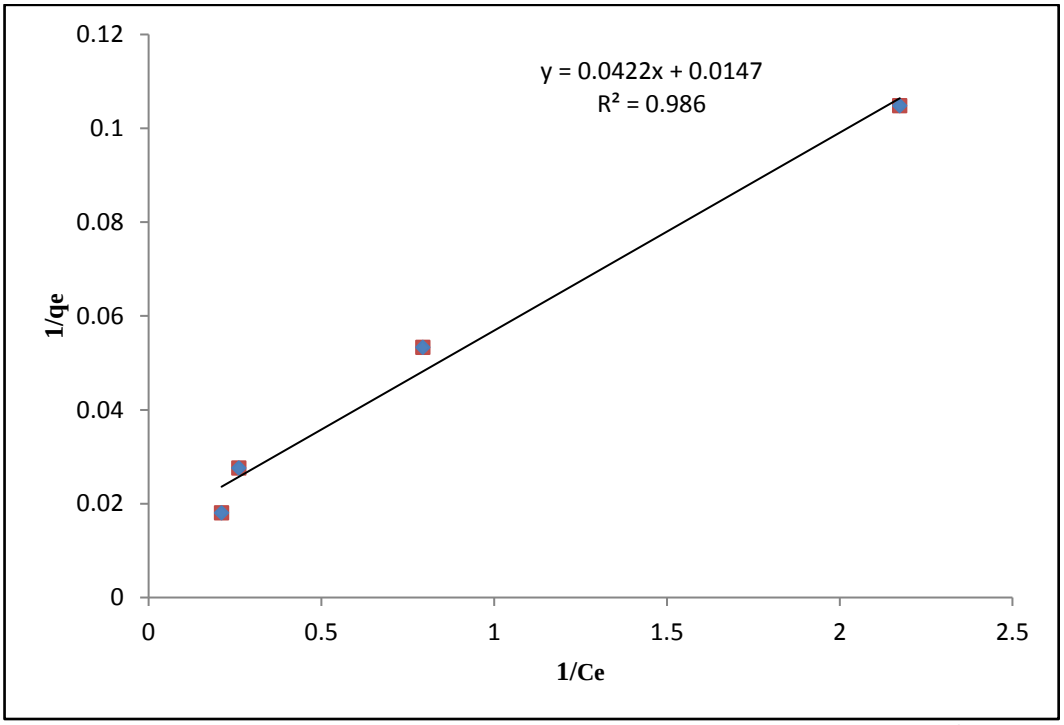

Figure 23: Langmuir Adsorption Isotherm with Plot of $1/q_e$ vs $1/c_e$ and R^2 0.986

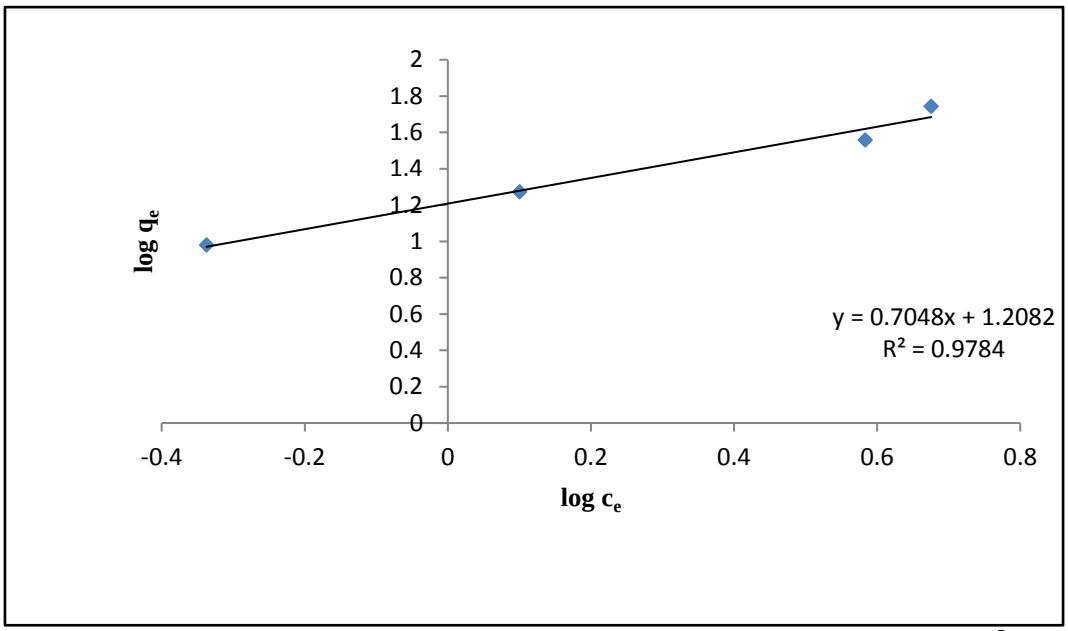

Figure 24: Freundlich Adsorption Isotherm with Plot of log q_e vs log c_e and R^2 0.9784

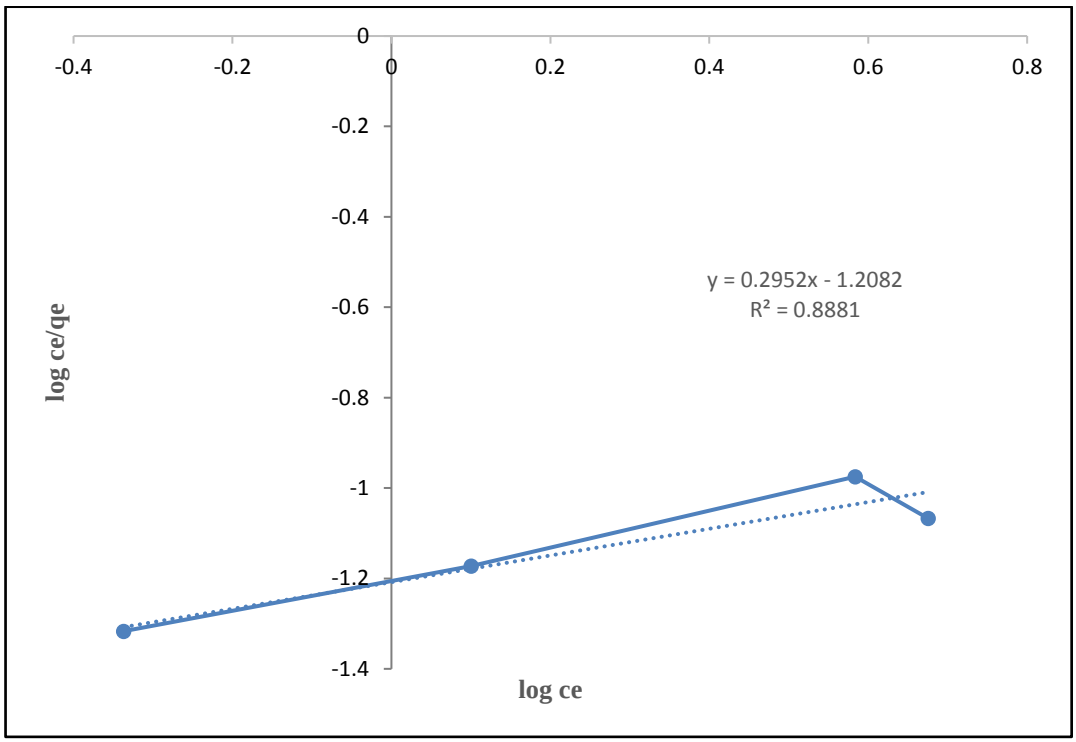

Figure 25: Redlich-Peterson Adsorption Isotherm with Plot of log c_e/q_e vs log c_e and R^2 0.8881

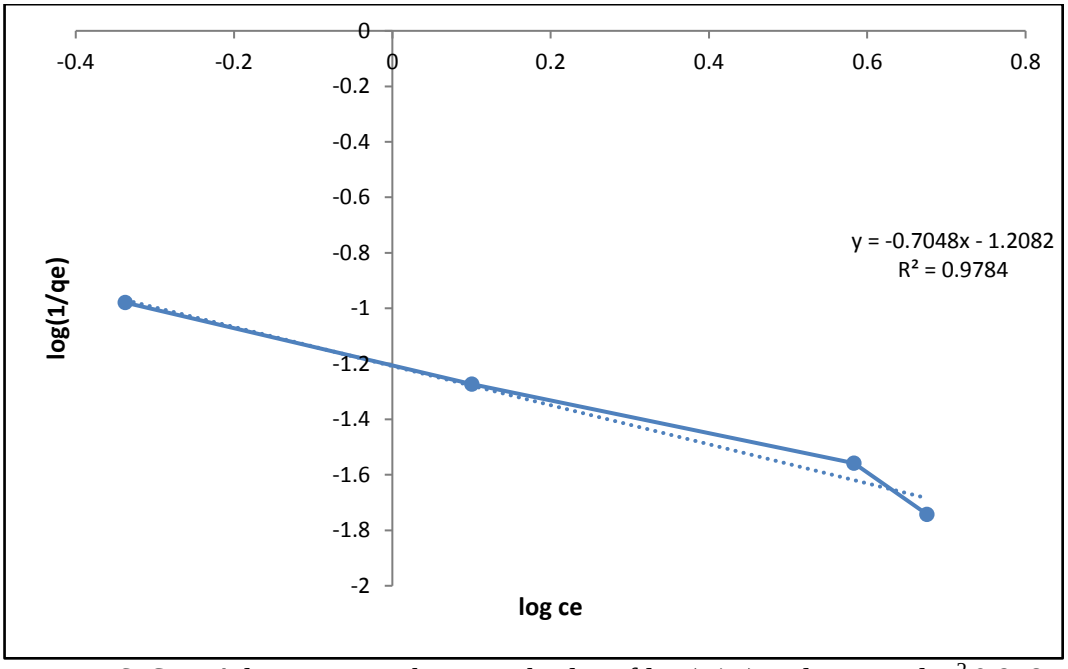

Figure 26: Sips Adsorption Isotherm with Plot of $\log(1/q_e)$ vs $\log c_e$ and R^2 0.9784

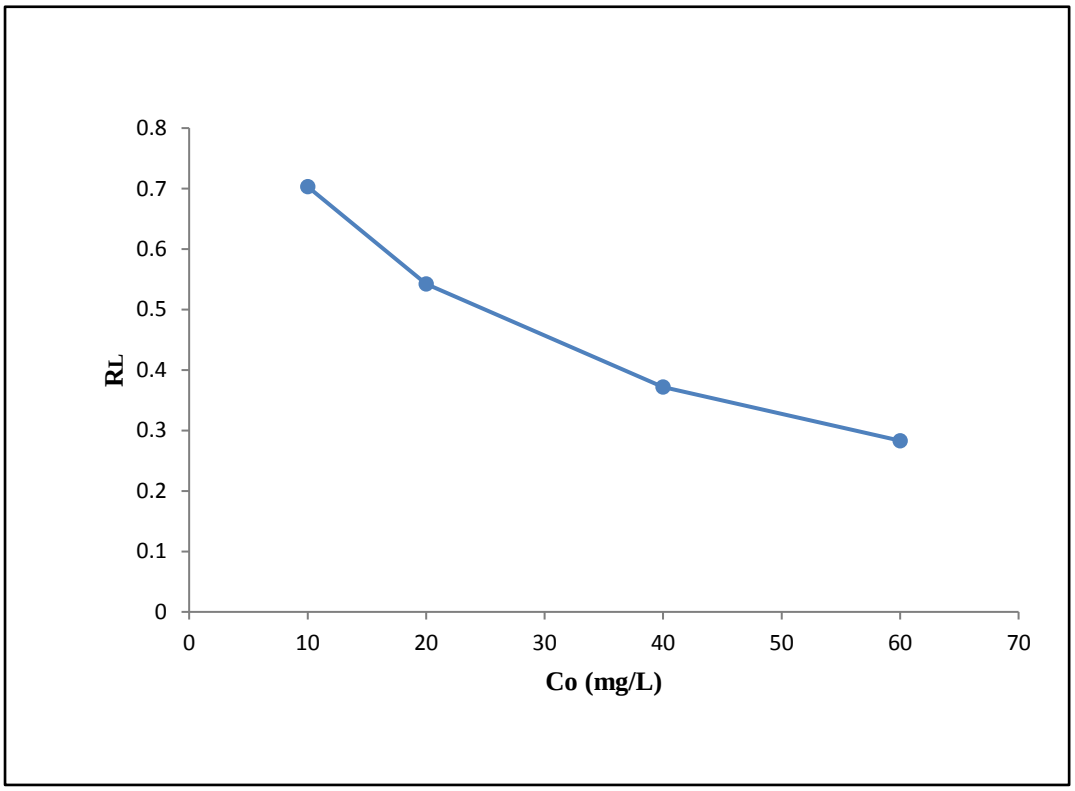

Figure 27: Separation Factor R_L Versus the Initial MB Dye Concentration at 298K.

3.7 Effect of Time and Adsorption Kinetics

The effect of contact time of the adsorbent with MB was studied and from Figure 28 it can be seen that qe increases with rise in contact time for the decolorization of MB until equilibrium is achieved. The optimum time was attained at 1440 minutes thereafter the percentage dye adsorption remained fairly constant. Amount of MB dye removed was established to be 97%, this showed that VCS-CT-g-PAAm hydrogel has excellent dye adsorption capacity.

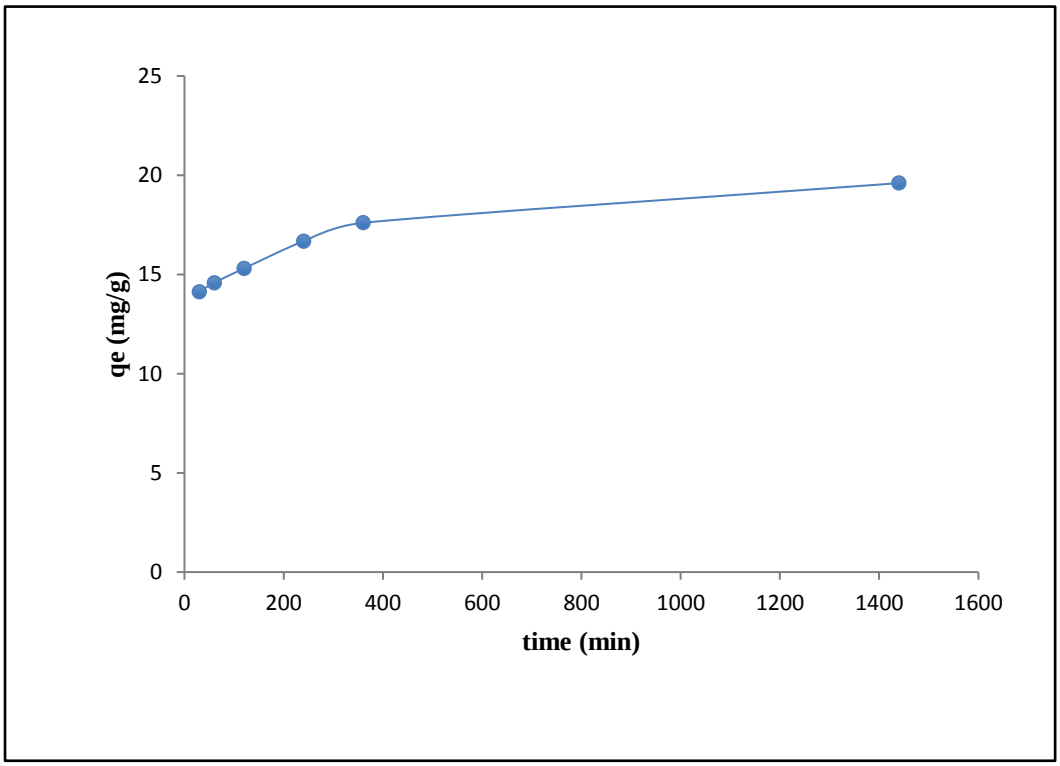

Figure 28: Effect of Time on the Adsorption of MB onto VCS-CT-g-PAAm Hydrogel

The absorption kinetics was studied with a contact time range of 30-1440 minutes. Four kinetic models (Pseudo first order (PFO), Pseudo second order (PSO), Elovich model and Boyd model) were used to fit the experimental data and propose a mechanism for the adsorption process. Figure 29, 30, 31 and 32 depicts the PFO, PSO, Elovich and Boyd model respectively. The correlation coefficient (R^2) as given in

Table 5, shows that the experimental data best fits into PFO and PSO model, though the R^2 of PSO was slightly higher than that of PFO.

Experimental data fitting into PFO, PSO model and negative value of ΔH^o suggests that the adsorption process is phyisorption which entails the physical interaction between the ionic species of the adsorbent and MB. To get further information regarding the mechanism of the sorption process, the experimental data was fitted into Body kınetıc model, from Figure32 it can be seen that the straight does not pass through the origin therefore film diffusion or bulk mass transport mechanism was suggested for the sorption process. This suggested sorption mechanism may be attributed to electrostatic interaction between the VCS-CT-g-PAAm hydrogel surface and the cationic MB dye molecules (Elkady et al. 2016). A subjective comparison between chitosan derivative hydrogels for the removal of dye pollutants and the present study is presented in Table 6.

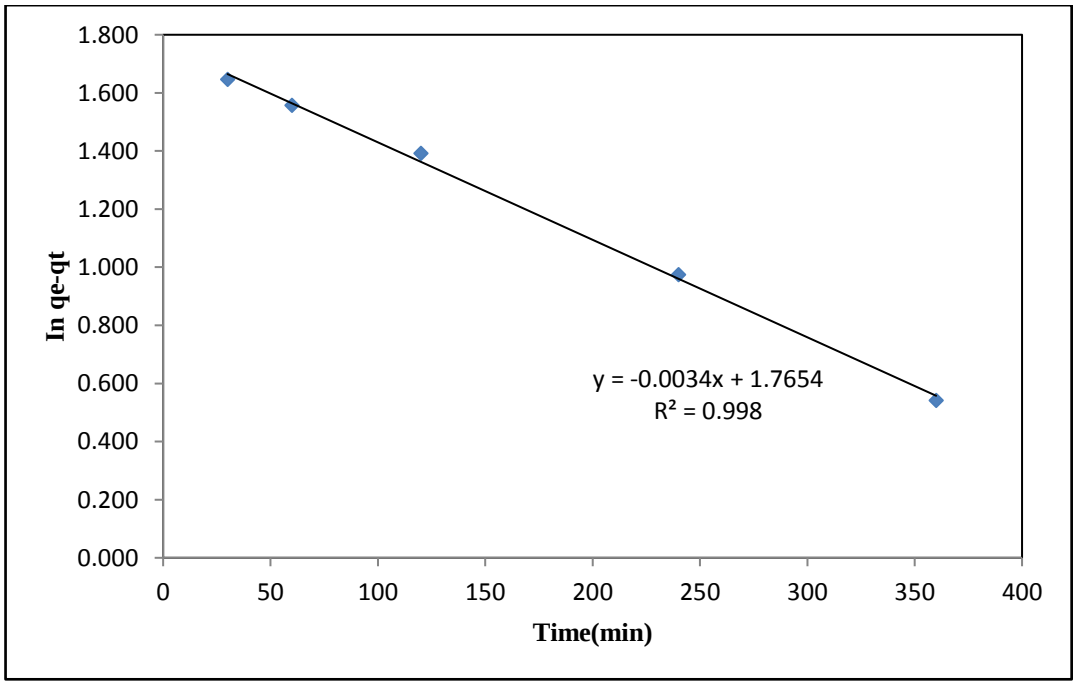

Figure 29: Pseudo-first-order Kinetics for the Adsorption of MB onto VCS-CT-g-PAAm Hydrogel

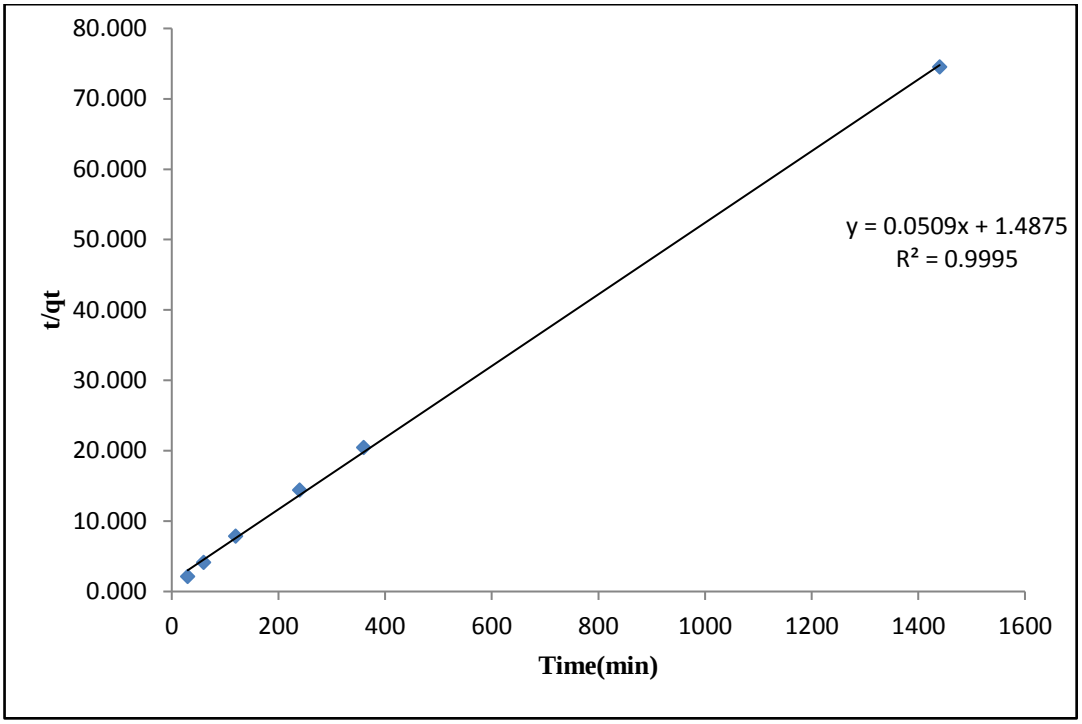

Figure 30: Pseudo-second-order Kinetics for the Adsorption of MB onto VCS-CT-g-PAAm Hydrogel.

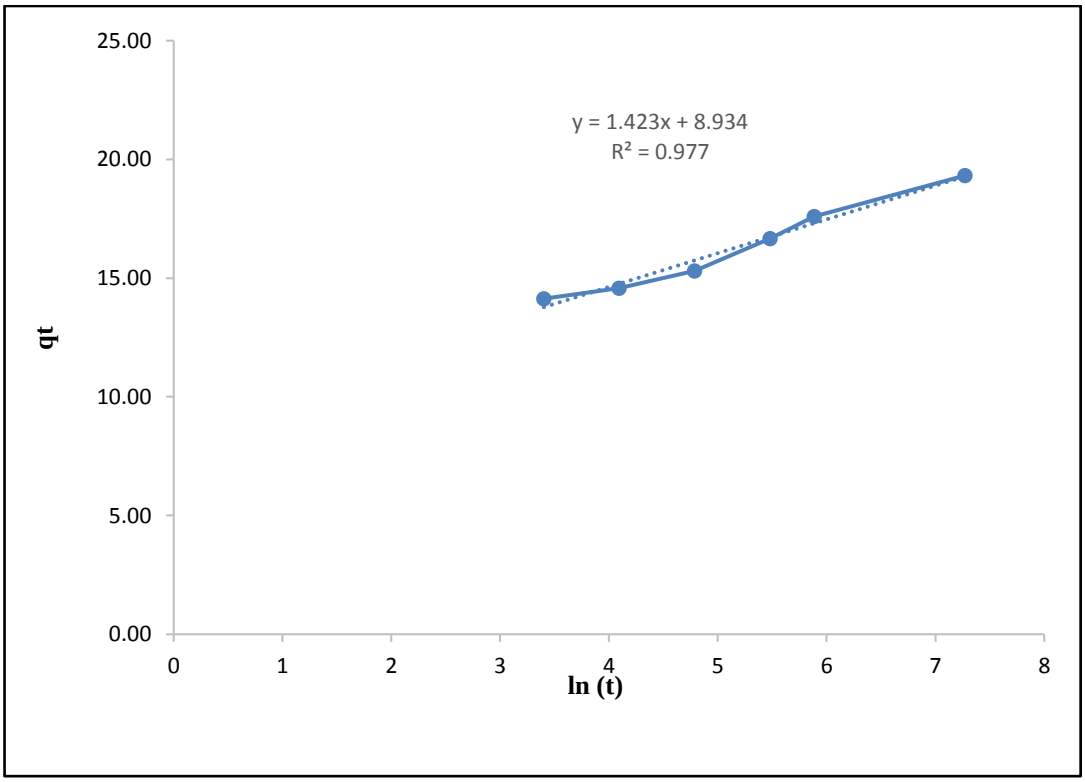

Figure 31: Elovich's Kinetic Model for MB Adsorption onto VCS-CT-g-PAAm

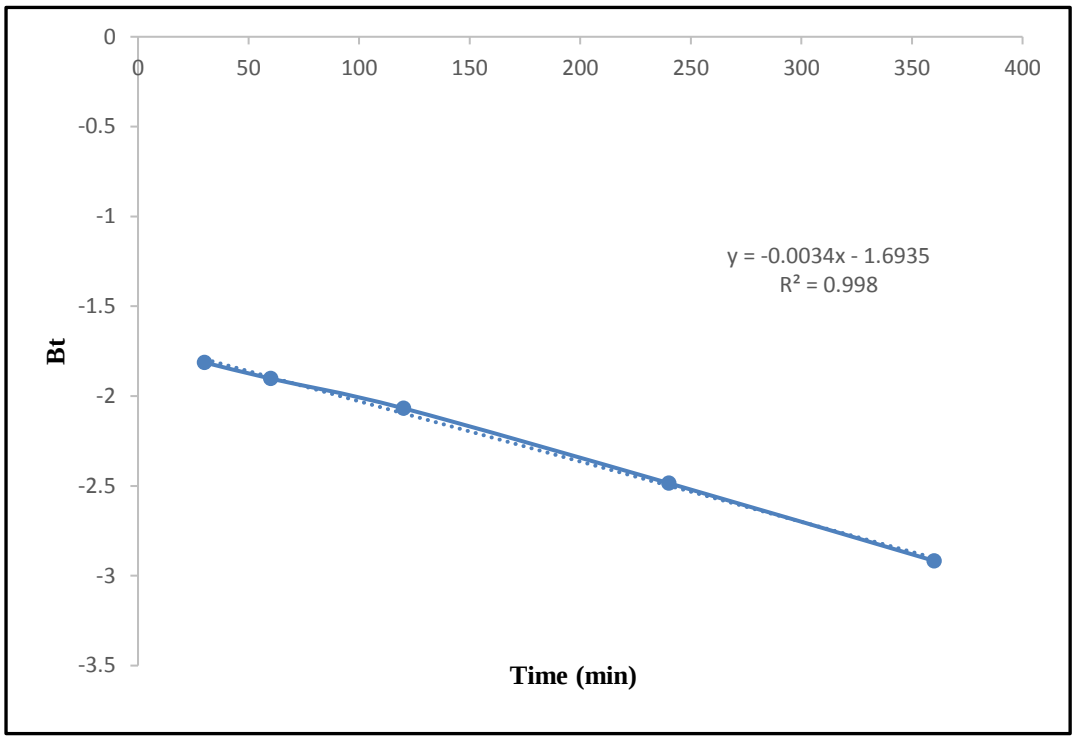

Figure 32: Boyd Kinetic Model for MB Adsorption onto VCS-CT-g-PAAm

Table 5: Kinetic constant for the sorption of MB onto Hydrogel

Kinetic Model	Parameter	Value
Pseudo first order model	K_1 (min^{-1}) R^2 q_e (mg/g)	0.0034 0.998 96.29
Pseudo second order model	K_2($gmg^{-1}min^{-1}$) R^2 q_e (mg/g)	0.672 0.999 98.29
Elovich model	B (g/mg) R^2	0.702 0.977
Boyd model	R^2	0.998

3.8 Thermodyniamc Parameters

The thermodynamics parameters, Gibbs free energy (ΔG^o), enthalpy (ΔH^o), entropy (ΔS^o) for the adsorption of MB onto VCS-CT-g-PAAm hydrogel were gotten using the Vant Hoof plots as can be seen in Figure31 and the values displayed in Table 6.

The negative values of ΔG^o at all temperatures (25-50 ^oC) shows that the adsorption of MB onto VCS-CT-g-PAAm hydrogel was a sponteneous process and thermodynamically favourable reaction (Kolodynska et al 2012). The negative value of ΔH^o obtained from this studies -2.722 KJ/mol indicates that the adsorption process is exothermic which is confirmed form Vant Hoff plot (Figure33). The positive values of ΔS^o at the measured temperatures shows increased randomness at the junction of the liquid/solid adsorption process, indicating excellent affinity for the VCS-CT-g-PAAm hydrogel towards MB dye (Venkata Ramana et al. 2012).

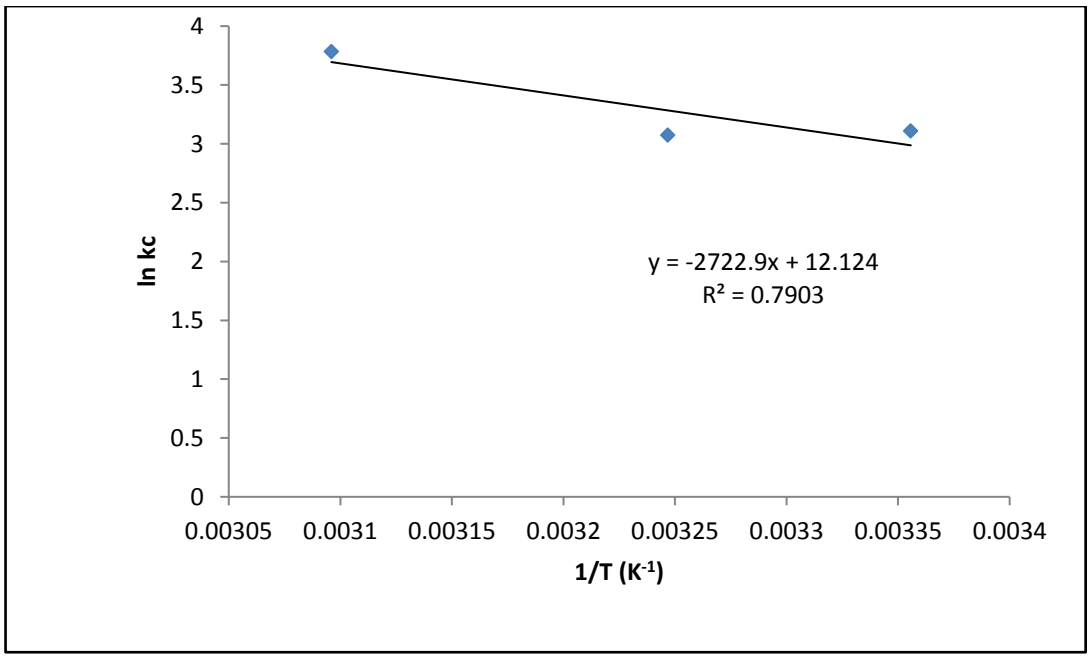

Figure 33: Vant Hoff Plot of ln kc vs 1/T Showing an Exothermic Process for Adsorption of MB onto VCS-CT-g-PAAm Hydrogel.

Table 6: Thermodynamic Parameters for Adsorption of MB onto Hydrogels

T (K)	ΔG^o (KJ/mol)	ΔH^o (KJ/mol)	ΔS^o (J/mol K)
298	-7.73	-2.72	16.72
308	-7.90		16.71
323	-10.19		23.02

3.9 Swelling Studies of VCS-CT-g-PAAm hydrogel

3.9.1 Effect of Time on Swelling Ratio

The effect of time on percentage swelling of the hydrogel was studied. The % swelling was 1176% after 1440 minutes at pH 9 as can be seen in Figure 34. The VCS-CT-g-PAAm swells more than 11 times its normal size when inserted into aqueous medium.

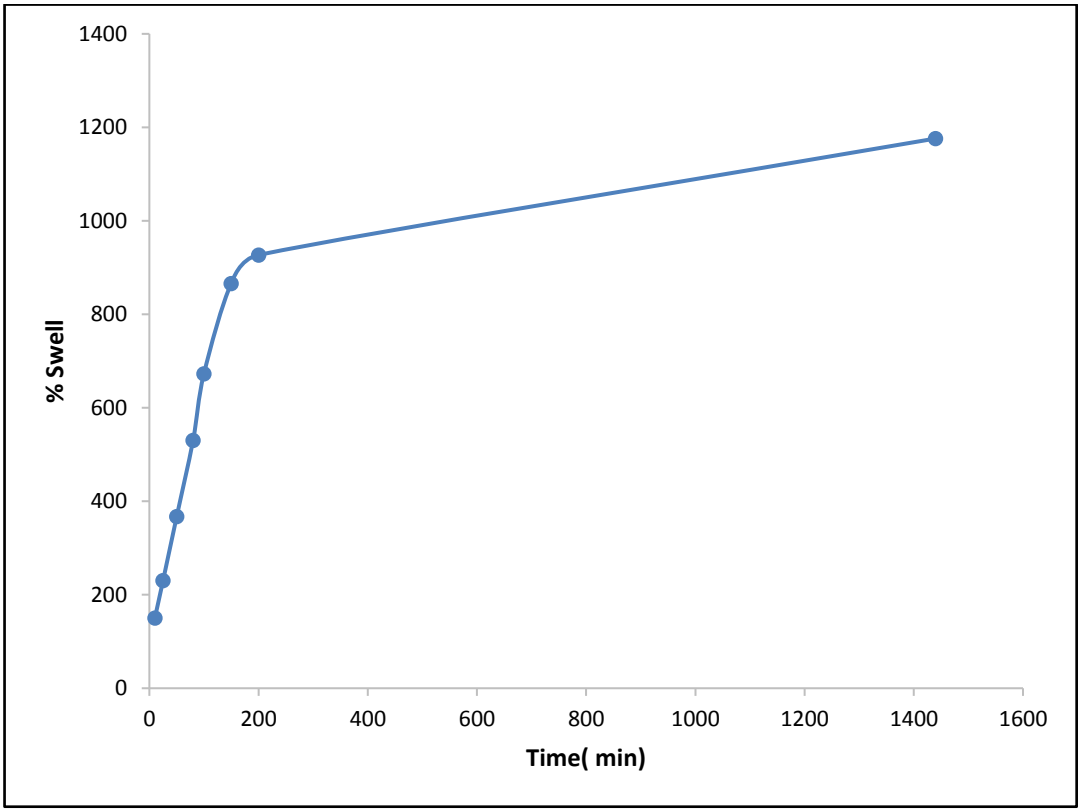

Figure 34: Effect of Time on % Swelling at pH 9.

3.9.2 Effect of pH on Swelling Ratio

VCS-CT-g-PAAm is pH sensitive and the swelling ratio increases as the pH increases. The maximum swelling ratio was obtained at a pH of 9, this can be seen from Figure (35), Figure (36) and Figure (37). The VCS-CT-g-PAAm has a higher swelling percentage in basic medium as compared to acidic medium.

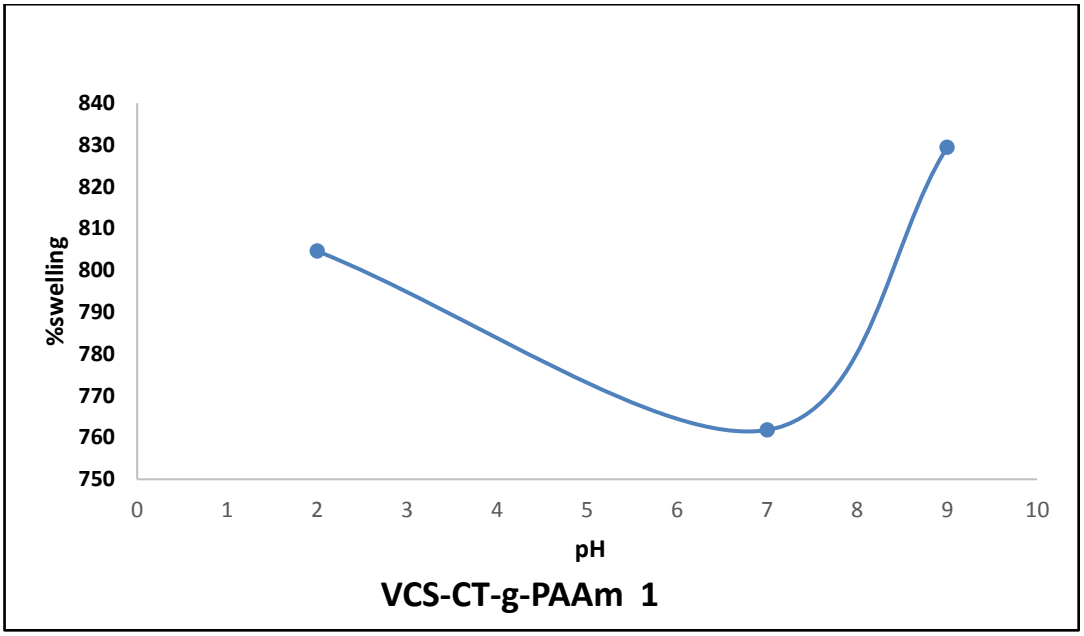

Figure 35: Swelling Percentage vs pH VCS-CT-g-PAAm1

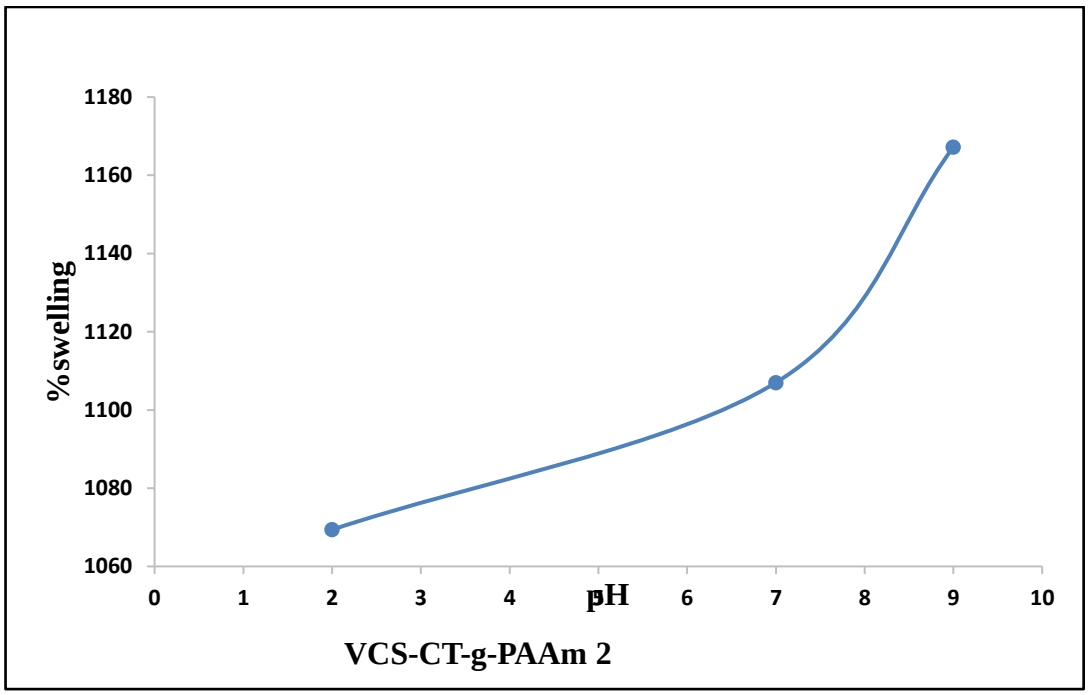

Figure 36: Swelling Percentage vs pH VCS-CT-g-PAAm2

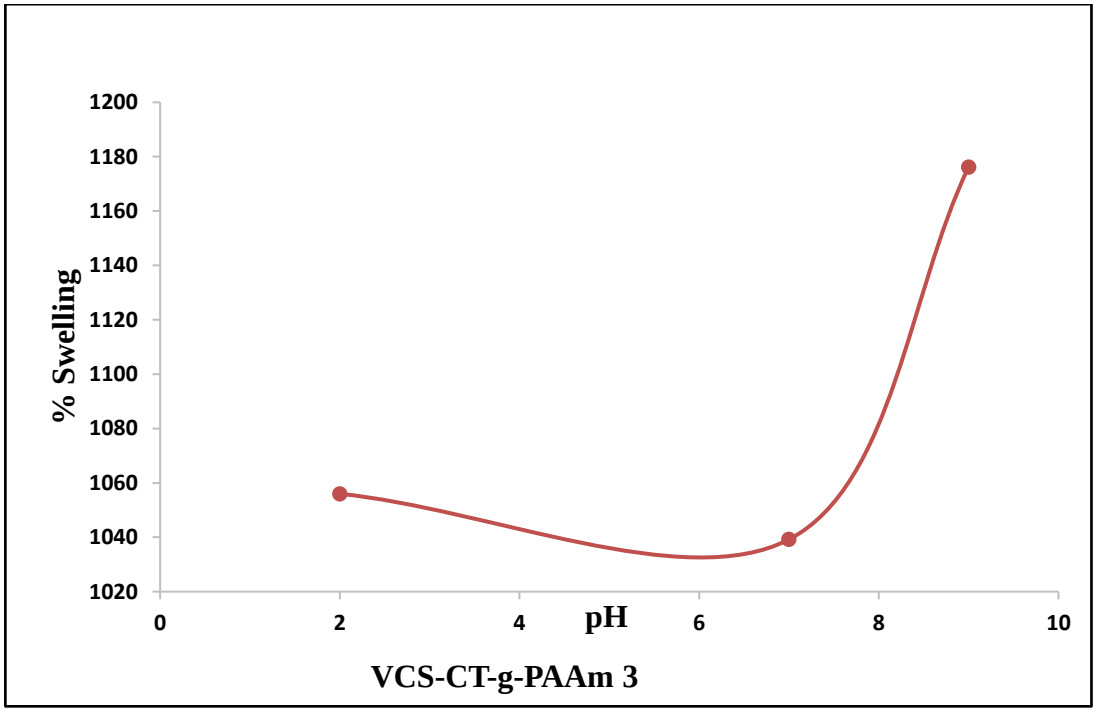

Figure 37: Swelling Percentage vs pH VCS-CT-g-PAAm3

3.10 Effect of Monomer Ratio Concentration on Percentage Gelation

Tab. 7 show the effect of monomer ratio, i.e acrylamide. The percentage gelation (GP) increases as the monomer concentration ratio changes and reaches a optimal value of 850% for a ratio of 0.1:0.9. The excess of monomer molecules on chitosan backbone inhibits further gelation.

Table 7: Concentration of VCS-CT, AAm, Crosslinker, Initiator in relation to gelation time, hydrogels weight and gelation percentage.

Sample	VCS-CT (g)	AAm monomer (g)	MBA crosslinker (g)	APS initiator (g)	Gelation Time (min)	Hydrogels weights (g)	Gelation %
A	0.1	0.9	0.05	0.05	2.5	0.95	850
B	0.1	0.7	0.05	0.05	3	0.81	710
C	0.1	0.5	0.05	0.05	7	0.675	575
D	0.1	0.3	0.05	0.05	9	0.444	344
E	-	0.3	0.05	0.05	1	0.319	219

3.11 Antibacterial studies of VCS-CT-g-PAAm hydrogel

As can be seen in Figs. 38 and 39 the VCS-CT-g-PAAm hydrogel exhibited a high percentage killing against *S. Aureus and E. Coli*, more than 99.9% after 24 h. The antibacterial activity of the hydrogel can be attributed to the presence of unsubstituted cationic amino groups on VCS-CT-g-PAAm which interacts with the bacterial cell wall. These finding is in sync with other reports on chitosan derivative against gram positive and gram negative bacteria (Xin et. al 2016; Kumar et. al 2018).

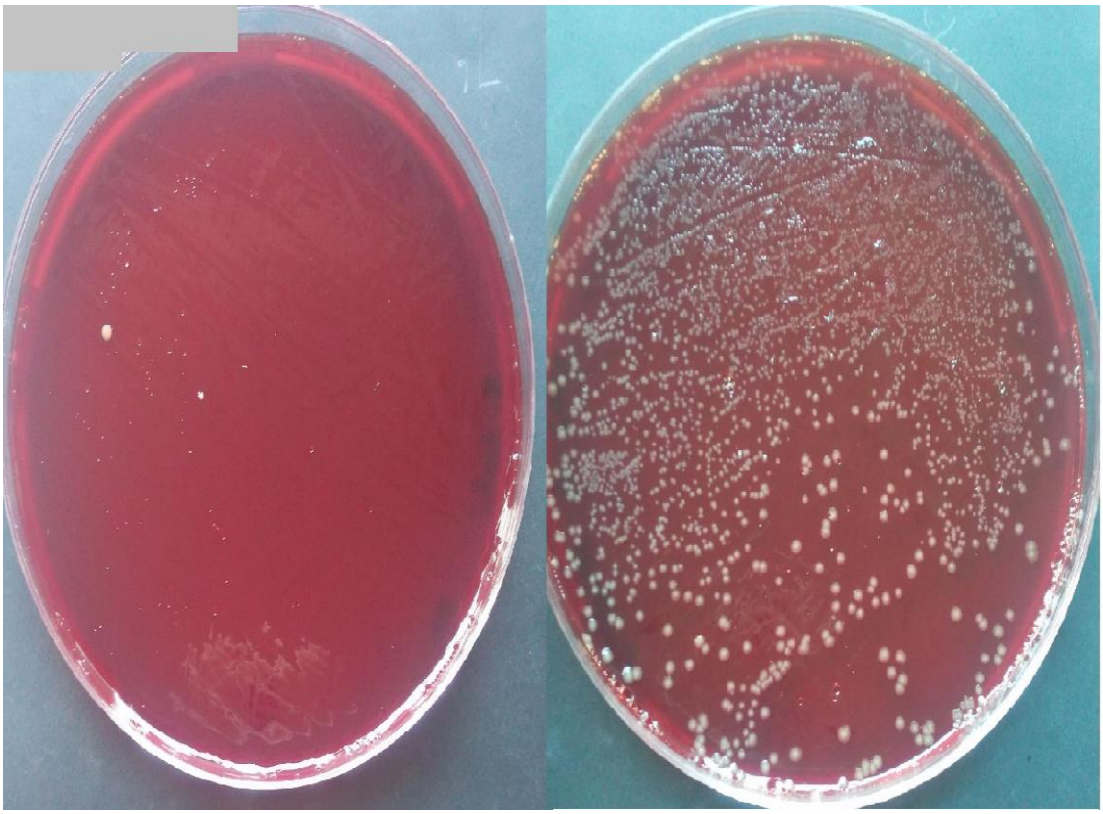

Figure 38: Antibacterial Activity of Hydrogel Prepared by VCS-CT-g-PAAm Against *E. coli* after 8hr Contact (Left Dish: *E.coli* + Hydrogel. Right Dish: *E.coli* Control)

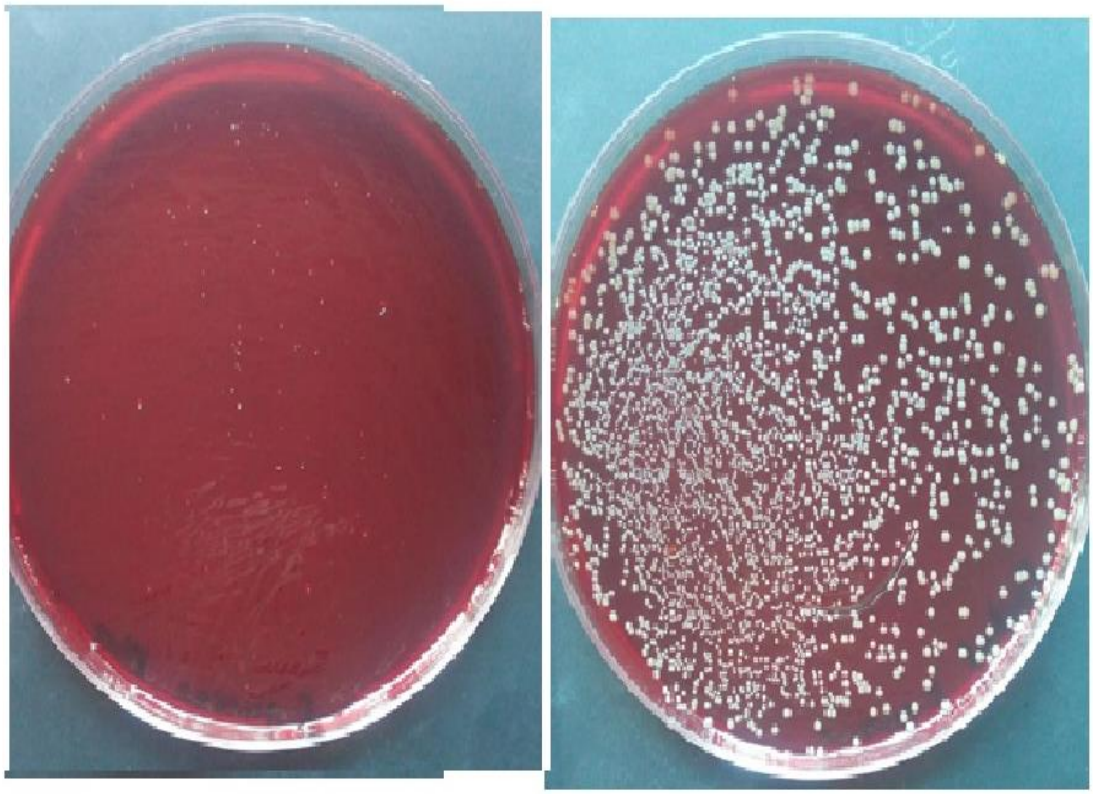

Figure 39: Antibacterial Activity of Hydrogel Prepared by VCS-CT-g-PAAm Against *S. aureus* after 8hr Contact (Left Dish: *S.aureus* + Hydrogel. Right Dish: *S.aureus* Control)

3.12 Comparative Analysis of VCS-CT-g-PAAm with Similar Hydrogels

The comparative analysis of VCS-CT-g-PAAm against other corresponding hydrogels showed similar trends in respective to adsorption capacity, pH, isotherm modelling and kinetic modelling. VSC-CT-g-PAAm was found to possess a higher adsorption capacity in comparison to other similar hydrogels (Table 8).

Table 8: VCS-CT-g-PAAm hydrogel adsorption kinetics and mechanism of pollutants in comparison with other similar hydrogels

Hydro-gel	Pollu-tant	Adsorp-tion capacity $q_{(max)}$	t	pH	Initial Pollutant concen-tration	Isoth-erm model	Kinetic model	Adsorp-tion mechani sm	Referen-ces
CS/PAN	RB	21.90 mg/g	240 min	7.0	100 mg/L	Lang-muir	PSO	Hydro-gen bonding	(Al-Mubaddel et al. 2015)
NaAlg/I A	MB	9.16 mg/g	5 h	8.0	80 mg/L	Freund-lich	PSO,PF O, IPD	Ion Exchange	(Mahmou d et al. 2014)
PAA-AAM/a mylose	Crystal Violet	28.60 mg/g	3 days	7.4-8	50 mg/L	Lang-muir	PSO	Electro-static and hydro-phobic interact-tion	(Li 2010)
FCBAC	MB	65.31 mg/g	90 min	8	70 mg/L	Lang-muir	PSO, IPD	Physico-chemical interact-tion	(Pathania et al. 2013)
VCS-CT-g-PAAm	MB	93.45 mg/g	24 h	12	100 mg/L	Lang-muir	PSO, Boyd	Film diffusion	This study

CS/PAN: Chitosan-graft-poly(acrylonitrile) hydrogel
NaAlg/IA: Sodium alginate-graft-icotonic acid hydrogel
PAA-AAM-amylose: Poly(acrylic acid)-polyacrylamide-graft-amylose hydrogel
FCBAC: Ficus carica bast activated carbon
VSC-CT-g-PAAm: Chitosan-poly(vinyltrichlorosilane)-graft-polyacrylamide hydrogel
RB: Rhodamine B
MB: Methylene blue
PFO: Pseudo first order
PSO: Pseudo second order
IPD: Inter particle diffusion

Chapter 4

CONCLUSION

A water-soluble chitosan-g-poly (trichlorovinylsilane) (CT-g-VTCS) film was successfully synthesized and its functional groups, surface morphology and crystalline nature were confirmed by FTIR, SEM and X-ray diffraction analyses, respectively. The results showed that CT-g-VTCS (MIC: 39–78 μg/mL) exhibited potentially higher antibacterial activity against *S. aureus* and *E. coli* cells compared to chitosan alone (156 μg/mL), due to its larger surface area, presence of strong electron-withdrawing group (–Cl–) and improved water solubility. The time-kill analysis indicated that the exposure of 10^7 CFU/mL bacteria cells to 0.325 mg/mL of CT-g-VTCS gave a ~0.08 $\log_{10}$ reduction (>99.9% kill rate). In addition, the inhibition zone of the CT-g-VTCS (23 mm) against *S. aureus* was larger than that of chitosan (5.4 mm). Collectively, results herein suggest the potential application of CT-g-VTCS as an efficient water-soluble antibacterial agent, further necessitating future studies to verify its exact reaction mechanism.

Prepared by VCS-CT-g-PAAm hydrogels were successfully tested for their swellability in acidic, basic and neutral medium. The hydrogels were found to exhibit high swelling ratio in basic medium. The antibacterial test of the hydrogels showed enhanced activity against *S.aureus and E.coli*. The adsorption studies for VCS-CT-g-PAAm hydrogel showed dependence on the pH medium of the MB dye used. The thermodynamic study predicts that the adsorption process was exothermic. The

experimental data fitted the Langmuir isotherm and the adsorption process followed a pseudo second order kinetics. The suggested mechanism for the sorption process was film diffusion or bulk mass transport mechanism by Boyd kinetic model plot.

Importantly, VCS-CT-g-PAAm hydrogel can adsorb MB dye from aqueous solution and can find application in waste water treatment and has potential application in the field of biomedical engineering.

REFERENCES

Abureesh MA., Oladipo AA., Gazi M. (2016) Facile synthesis of glucose-sensitive chitosan–poly (vinyl alcohol) hydrogel: Drug release optimization and swelling properties. *Int J Biol Macromol* 90: 75–80. https://doi.org/10.1016/j.ijbiomac.2015.10.001.

Abureesh MA, Oladipo AA, Mizwari ZM, Berksel E (2018) Engineered mixed oxide-based polymeric composites for enhanced antimicrobial activity and sustained release of antiretroviral drug. *Int J Biol Macromol* 116: 417–425. https://doi.org/10.1016/j.ijbiomac.2018.05.065.

Ahmad N, Ahmad R, Alam MA, Ahmad FJ, et al. (2019) Daunorubicin oral bioavailability enhancement by surface coated natural biodegradable macromolecule chitosan based polymeric nanoparticles. *Int J Biol Macromol* 128:825–838. https://doi.org/10.1016/j.ijbiomac.2019.01.142.

Ahmad N, Ahmad R, Naqvi AA, Alam MA, et al. (2016) Rutin-encapsulated chitosan nanoparticles targeted to the brain in the treatment of Cerebral Ischemia. *Int J Biol Macromol* 91:640–55. https://doi.org/10.1016/j.ijbiomac.2016.06.001.

Ahmad N, Al-Subaie AM, Ahmad R, et al. (2019) Brain-targeted glycyrrhizic-acid-loaded surface decorated nanoparticles for treatment of cerebral ischaemia and its toxicity assessment, *Artif Cells Nanomed Biotechnol* 47: 475–490 https://doi.org/10.1080/21691401.2018.1561458.

Aleanizy FS, Alqahtani FY, Shazly G, Alfaraj R, Alsarra I, Alshamsan A, Abdulhady HG (2018) Measurement and evaluation of the effects of pH gradients on the antimicrobial and antivirulence activities of chitosan nanoparticles in Pseudomonas aeruginosa. *Saudi Pharm J* 26: 79–83. https://doi.org/10.1016/j.jsps.2017.10.009.

Al-Mubaddel FS, Aijaz MO, Haider S, Haider A, Almasry WA, Al-FAtesh AS (2015) Synthesis of chitosan based semi –IPN hydrogels using epichlorohydrine as crosslinker to study the adsorption kinetics of rhodamine B. *Desalin Water Treat* 57:17523-17536.

Alqahtani FY, Aleanizy FS, El Tahir E, Alquadeib BT, Alsarra IA, Alanazi JS, Abdelhady HG (2019) Preparation, characterization, and antibacterial activity of diclofenac-loaded chitosan nanoparticles. *Saudi Pharm J* 27: 82–87. https://doi.org/10.1016/j.jsps.2018.08.001.

Al-qudah YHF, Mahmoud GA, Abdel Khalek MA (2014) Radiation crosslinked poly (vinyl alcohol)/acrylic acid copolymer for removal of heavy metal ions from aqueous solutions. Journal of Radiation *Research and Applied Sciences*7(2):135-14, https://doi.org/10.1016/j.jrras.2013.12.008.

Anderson MA, Rubin AJ (1981) Adsorption of Inorganic at Solid Liquid Interfaces; Ann Arbor Science Publishers: Ann Arbor, MI, Chapter 1.

Anwar J, Shafique U, Waheed Z, Salman M, Dar A, Anwar S (2010) Removal of Pb(II) and Cd(II) from water by adsorption on peels of banana. *Bioresour Technol* 101:1752. doi:10.1016/j.biortech.2009.10.021.

Aranaz I, Mengı bar M, Harris R, Pan˜os I, Miralles B, Acosta N, Gemma G, Heras A (2009) *Curr Chem Biol* 3(2):203–230.

Asgharzadehahmadi SA, Khairuddin Imn, Norulfairuz D, Zaidel A, Eko S (2013) Synthesis and Characterization of Polyacrylamide Based Hydrogel Containing Magnesium Oxide Nanoparticles for Antibacterial Applications. *Universiti Technologi Malaysia*. https://pdfs.semanticscholar.org/a7d5/25f935a4f3f1fc3030e0069059dadcf0825f.pdf.

Ayawei N, Ekubo AT, Wankasi D, Dikio ED (2015) Adsorption of congo red by Ni/Al-CO3: equlibrium, thermodynamic and kinetic studies. *Oriental Journal of Chemistry* 31(30):1307-1318.

Bakshi PS, Selvakumar D, Kadirvelu K, Kumar NS (2018) Comparative study on antimicrobial activity and biocompatibility of N-selective chitosan derivatives. *React Funct Polym* 124: 149–155. https://doi.org/10.1016/j.reactfunctpolym.2018.01.016.

Bharathi D, Ranjithkumar R, Chandarshekar B, Bhuvaneshwari V (2019) Preparation of chitosan coated zinc oxide nanocomposite for enhanced antibacterial and

photocatalytic activity: As a bionanocomposite. *Int J Biol Macromol* 129: 989–996. https://doi.org/10.1016/j.ijbiomac.2019.02.061.

Bhattacharya A and Misra BN (2004) Grafting: a versatile means to modify polymers. Techniques, factors and applications. *Progress in polymer science*. doi:10.1016/j.progpolymsci.2004.05.002.

Bhatti HN, Akhtar N, Saleem N (2012) Adsorptive removal of methylene blue by low cost citrus sinensis bagasse: Equilibrium, kinetic and thermodynamic characterization. *Arab J Sci Eng* 37:9-18.

Bhatti HN, Safa Y (2012) Removal of anionic dyes by rice milling waste from synthetic effluents: Equilibrium and thermodynamics studies. *Desal Water Treat* 48:267-277.

Bhuiyan MR, Shaid A, Khan MA (2014) *Chem Mater Eng* 2(4):96–100.

Blondeau JM, Shebelski SD, Hesje CK (2015) Killing of Streptococcus pneumoniae by azithromycin, clarithromycin, erythromycin, telithromycin and gemifloxacin using drug minimum inhibitory concentrations and mutant prevention concentrations. *Int J Antimicrob Agents* 45: 594–599. https://doi.org/doi:10.1016/j.ijantimicag.2014.12.034.

Boributh S, Chanachai A, Jiraratananon R. (2009) *Journal of Membrane Science*. 342:97-104.

Brouers F, Al-Musawi TJ (2015) On the optimal use of isotherm models for the characterization of biosorption of lead onto algae. *Journal of Molecular Liquids* 212:46-51.

Buenger D, Topuz F, Groll J (2012) Hydrogels in sensing applications. *Prog Polym Sci* 37(12):1678–719.

Cao W, Yue L, Wang Z (2019) High antibacterial activity of chitosan–molybdenum disulfide nanocomposite. *Carbohyd Polym* 215: 226–234. https://doi.org/10.1016/j.carbpol.2019.03.085.

Casal E, Montilla A, Moreno FJ, Olano A, Corzo N (2006) Use of Chitosan for Selective Removal of β-Lactoglobulin from Whey. *Journal of Dairy Science*. 89:1384-1389.

Chatterjee S, Lee DS, Lee MW, Woo SH (2009) Enhanced adsorption of Congo red from aqueous solutions by chitosan hydrogel beads impregnated with cetyl trimethyl ammonium bromide. *Bioresour Technol* 100: 2803-2809.

Chen C (2012) Evaluation of equilibrium sorption isotherm equations. *Open Chemical Engineering Journal* 7:24-44.

Chen X, Chen G, Chen L, Chen Y, Lehmann J, Mcbridge MB, Hay AG (2011) Adsorption of copper and zinc by biochars produced from pyrolysis of hardwood

and corn straw in aqueous solution. *Bioresourc Technol* 102:8877-8884. doi:10.1016/j.biortech.2011.06.078.

Chen Y, Li J, Li Q, Shen Y, Ge Z, Zhang W, Chen S (2016) Enhanced water solubility, antibacterial activity and biocompatibility upon introducing sulfobetaine and quaternary ammonium to chitosan. *Carbohyd Polym* 143: 246–253. https://doi.org/doi:10.1016/j.carbpol.2016.01.073.

Chylińsk M, Kaczmarek H, Burkowska-But A (2019) Preparation and characteristics of antibacterial chitosan films modified with N-halamine for biomedical application. *Colloids Surf B* 176: 379–386. https://doi.org/10.1016/j.colsurfb.2019.01.013.

Correia VG, Coelho M, Barroso T, Raje VP, Bonifacio VDB, Casimiro T, Pinho MG, Aguiar-Ricardo A (2013) *Biofouling* 29:273-282.

Dang Q, Liu K, Liu C, Xu T, Yan J, Yan F, Cha D, Zhang Q, Cao Y (2018) Preparation, characterization, and evaluation of 3,6-O-N-acetylethylenediamine modified chitosan as potential antimicrobial wound dressing material. *Carbohyd Polym* 180: 1–12. https://doi.org/10.1016/j.carbpol.2017.10.019.

Daraei H, Mittal A, Noorisepehr M, Mittal J (2013) Separation of chromium from water samples using eggshell powder as a low-cost sorbent: Kinetic and thermodynamic studies. *Desal Water Treat* doi:10.1080/19443994.2013.837011.

Davoundinejad M, Gharbanian SA (2013) Modelling of adsorption isotherm of benzoic compounds onto GAC and introducing three new isotherm models using new concept of adsorption effective surface (AEC). *Academic journals* 18(46):2263-2275.

Elkady MF, El-Aassar MR, Hassan HS (2016) Asorption Profile of Basic Dye onto Novel Fabricated Carboxylated Functionalized Co-Polymer Nanofibers. *Polymers* 8(5):177. doi:10.3390/polym8050177.

Elmorsi TM (2011) Equilibrium isotherms and kinetics studies of removal of methylene blue dye by adsorption onto miswak leaves as a natural adsorbent. *Journal of Environmental Protection* 2(6):817-827.

El-Shahawy AAG, El-Ela FIA, Mohamed NA, Eldine ZE, El Rouby WMA (2018) Synthesis and evaluation of layered double hydroxide/doxycycline and cobalt ferrite/chitosan nanohybrid efficacy on gram positive and gram negative bacteria. *Mater Sci Eng C* 91: 361–371. https://doi.org/10.1016/j.msec.2018.05.042.

Ferfera-Harrar H, Aiouaz N, Dairi N, Hadj-Hamou AS (2014) Preparation of chitosan-g-poly(acrylamide)/montmorillonite superabsorbent polymer composites: Studies on swelling, thermal, and antibacterial properties. *J Appl Polym Sci* 131(1) http://doi.wiley.com/10.1002/app.39747.

Foo KY, Hameed BH (2009) Insights into the modeling of adsorption isotherm systems. *Chemical Engineering Journal* 156:2-10.

Four Effective Processes To Treat Watewater (2018) Retrieved from https://eponline.com/Articles.

Gazi M, Shahmohammadi S (2012) Removal of trace boron from aqueous solution using iminobis-(propylene glycol) modified chitosan beads. *React Funct Polym* 72: 680–686. https://doi.org/10.1016/j.reactfunctpolym.2012.06.016.

Gita S, Ajmal H , Tanmoy GC (2017) Impact of Textile Dyes Waste on Aquatic Environments and its *Treatment. Environment and Ecology* 35(3C): 2349-2353.

Grade S, Eberhard J, Neumeister A, Wagener P, Winkel A, Stiesch M, et al. (2012) Serum albumin reduces the antibacterial and cytotoxic effects of hydrogel-embedded colloidal silver nanoparticles. *RSC Adv* 7190 http://xlink.rsc.org/?DOI=c2ra20546g.

Gritsch L, Lovell C, Goldmann WH, Boccaccini AR (2018) Fabrication and characterization of copper(II)-chitosan complexes as antibiotic-free antibacterial biomaterial. *Carbohyd Polym* 179: 370–378. https://doi.org/doi:10.1016/j.carbpol.2017.09.095.

Guler S, Ozseker EE, Akkaya A (2016) Developing an antibacterial biomaterial. *European Polym J* 84:326–337. https://doi.org/10.1016/j.eurpolymj.2016.09.031.

Guo AJ, Wang FH, Lin WT, Xu XF, Tang TT, Shen YY, et al., (2014) Evaluation of antibacterial activity of N-phosphonium chitosan as a novel polymeric

antibacterial agent. *Int J Biol Macromol* 67: 163–171. https://doi.org/doi:10.1016/j.ijbiomac.2014.03.024.

Halpenny GM, Steinhardt RC, Okialda KA, Mascharak PK (2009), Characterization of pHEMA-based hydrogels that exhibit light-induced bactericidal effect via release of NO. *J. Mater. Sci.: Mater. Med.* 20(11):2353-60. doi: 10.1007/s10856-009-3795-0.20.

Hameed BH (2009) Spent tea leaves: a new non-conventional and low-cost adsorbent for removal of basic dye from aqueous solutions. *J Hazard Mater* 161:753-759.

Ho YS, Mckay G (1999) Pseudo-second order model for sorption processes. *Process Biochemistry* 34:451-465.

Holback H, Yeo Y, Park K (2011) Hydrogel swelling behavior and its biomedical applications. *Biomedical Hydrogels* p. 3–24.

Ikeda T, Yamaguchi H, Tazuke S (1984), New polymeric biocides: synthesis and antibacterial activities of polycations with pendant biguanide groups. *Antimicrob. Agents Chemother*. 26(2): 139–144. doi: 10.1128/aac.26.2.139.

Islam S, Bhuiya MAR, Islam MN (2017) Chitin and Chitosan: Structure, Properties and Applications in Biomedical Engineering. *J Polym Environ* 25: 854–866. doi:10.1007/s10924-016-0865-5.

Jabeen SQ, Mehmood S, Tariq B, et al. (2011) Health impact caused by poor water and sanitation in district Abbottabad. *J Ayub Med Coll Abbottabad* 23(1):47-50.

Jin L, Bai R (2002) Mechanisms of lead adsorption on Chitosan/PVA hydrogel beads. *Langmui*r 18: 9765-9770.

Kajjumba GW, Emik S, Ongen A, Ozcan KH, Aydin S (2018) Modelling Of Adsorption Kinetic Processes-Errors, Theory and Application, *Advanced Sorption Process Applications*, Serpil Edebali doi:http://dx.doi.org/10.5772/intechopen.80495.

Karpuraranjith M, Thambidurai S (2017) Chitosan/zinc oxide-polyvinylpyrrolidone (CS/ZnO-PVP) nanocomposite for better thermal and antibacterial activity. *Int J Biol Macromol* 104:1753–1761. https://doi.org/10.1016/j.ijbiomac.2017.02.079.

Kaur S, Dhillon GS (2014) The versatile biopolymer chitosan: potential sources, evaluation of extraction methods and applications. *Critical Reviews in Microbiology* 40:155-175.

Kiseler AVC (1958) Vapour adsorption in the formation of adsorbate Molecule Complexes on the surface. *Kolloid Zhur* 20:338-348.

Kolodynska D, Wnetrzak R, Leahy JJ, Hayes MHB, Kwapinski W, Hubicki Z (2012) Kinetic and adsorptive characterization of biochar in metal ions removal. *Chem Eng J* 197:295-305 https://doi.org/10.1016/j.cej.2012.05.025.

Komata Y, Yoshikawa M, Tamura Y, Wada H, Shimojima A, Kuroda K (2016) Selective formation of alkoxychlorosilanes and organotrialkoxysilane with four different substituents by intermolecular exchange reaction. *Chem Asian J* 11: 3225–3233. https://doi.org/10.1002/asia.201601120.

Kong M, Chen XG, Xing K, Park HJ (2010) Antimicrobial properties of chitosan and mode of action: a state of the art review. *Int J Food Microbiol* 144: 51–63. https://doi.org/10.1016/j.ijfoodmicro.2010.09.012.

Kosemund K, Schlatter H, Ochsenhirt JL, Krause EL, Marsman DS, Erasala GN (2009) Safety evaluation of superabsorbent baby diapers. *Regul Toxicol Pharmacol* 53(2):81– 96.

Kumar D, Kumar P, Pandey J (2018) Binary grafted chitosan film: Synthesis, characterization, antibacterial activity and prospects for food packaging. *Int J Biol Macromol* 115:341-348.

Kurita K (2001) Prog Polym Sci 26(9):1921–1971.

Langmuir I (1916) The constitution and fundamental properties of solids and liquids. *J Am Chem Soc* 38:2221-2295.

Levan MD, Vermeulen T (1981) Binary Langmuir and Freundlich isotherms for ideal adsorbed solutions. *The Journal of Physical Chemistry* 85(22):3247-3250. doi:10.1021/j150622a009.

Li K, Guan G, Zhu J, Wu H, Sun Q (2019) Antibacterial activity and mechanism of a laccase-catalyzed chitosan–gallic acid derivative against Escherichia coli and Staphylococcus aureus. *Food Control* 96: 234–243. https://doi.org/10.1016/j.foodcont.2018.09.021.

Li S (210) Removal of crystal violet from aqueous solution by sorption into semi-interpenetrated networks hydrogels constituted of poly(acrylic acid-acrylamide-methacrylate) and amylose. *Bioresour Technol* 101:2197-2202.

Li S, Dong S, Xu W, Tu S, Yan L, Zhao C, et al (2018) Antibacterial Hydrogels. *Adv Sci* 5(5):1700527 http://doi.wiley.com/10.1002/advs.201700527.

Ma J, Zhou G, Chu L, Liu Y, Liu C, Luo S, Wei Y (2017) Efficient removal of heavy metal ions with an EDTA functionalized chitosan/polyacrylamide double network hydrogel. *ACS Sustain Chem Eng* 5:843-851.

Mahmood T, Saddique MT, Naeem A, Mustafa S, Dilara B, Raza ZA (2011) Cation Exchange Removal of Cd from Aqueous Solution by NiO. *J Hazard Mater* 185:824.

Mahmoud GA, Mohamed SF, Hassan HM (2014) Removal of methylene blue dye using biodegradable hydrogel and reusing in a secondary adsorption process. *J Desalin Water Treat* 54:1-12.

Merlusca IP, Matiut DS, Lisa G, Silion M, Gradinaru L. Oprea S, Popa IM (2018) Preparation and characterization of chitosan– poly(vinyl alcohol)–neomycin sulfate films. *Polym Bull* 75:3971–3986. https://doi.org/10.1007/s00289-017-2246-1.

Misra BN, Dogra R, Mehta IK (1980) Grafting onto cellulose V. Effect of complexing agents on Fenton's Reagent (Fe2+-H2O2) initiated grafting of poly (ethyl acrylate). *J Polym Sci Polym Chem* 18:749-752.

Mittal A, Jain R, Mittal J, Varshney S, Sikarwar S (2010) Removal of Yellow ME 7 GL from industrial effluent using electrochemical and adsorption techniques. *Int J Environ Pollut* 43(4):308-323.

Negahi Shirazi A, Imani M, Sharifi S (2011) Direct Condensation Reaction for Grafting of Polyethylene Glycol Monomethyl Ether on Poly(Methacrylic Acid-co-Methyl Methacrylate) for Application in Biomedical Engineering. *American Journal of Biomedical Engineering* doi: 10.5923/j.ajbe.20110101.03.

Ng JCY, Cheung WH, Mckay G (2002) Equilibrium studies of the sorption of Cu(II) ions onto chitosan. *Journal of Colloid and Interface Science* 225:64-74.

No HK, Meyers SP (1995) *J Aquat Food Prod Technol* 4(2):27–52.

Noreen S, Bhatti HN, Nausheen S, Sadaf S, Ashafaq M (2013) Batch and fixed bed adsorption study for the removal of Drimarine Black CL-B dye from aqueous

solution using a lignocellulosic waste, A cost effective adsorbent. *Ind Crop Prod* 50:568-579.

Ogugbue CJ, Sawidis T (2011) Bioremediation and Detoxification of Synthetic Wastewater Containing Triarylmethane Dyes by Aeromonas hydrophila Isolated from Industrial Effluent. *Biotechnology Research International*; DOI 10.4061/2011/967925.

Oladipo AA, Gazi M, Yilmaz E (2015) Single and binary adsorption of azo and anthraquinone dyes by chitosan-based hydrogel: Selectivity factor and Box-Behnken process design. *Chem Eng Res Design* 104: 264–279. https://doi.org/10.1016/j.cherd.2015.08.018.

Olgun A, Atar N (2012) Equilibrium, thermodynamic and kinetic studies for the adsorption of lead (II) and nickel (II) onto clay mixture containing boron impurity. *J Ind Eng Chem* 18(5):1751-1757.

Ozseker EE, Akkaya A (2016) Development of a new antibacterial biomaterial by tetracycline immobilization on calcium-alginate beads. *Carbohyd Polym* 151: 441–451. https://doi.org/10.1016/j.carbpol.2016.05.073.

Pan C, Qian J, Fan J, Guo H, Gou L, Yang H, Liang C (2019) Preparation nanoparticle by ionic cross-linked emulsified chitosan and its antibacterial activity. *Colloids Surf A* 568: 362–370. https://doi.org/10.1016/j.colsurfa.2019.02.039.

Parsons C, McCoy CP, Gorman SP, Jones DS, Bell SE, Brady C, McGlinchey SM (2009), Anti-infective photodynamic biomaterials for the prevention of intraocular lens-associated infectious endophthalmitis. *Biomaterials* 30(4):597-602. doi: 10.1016/j.biomaterials.2008.10.015.

Pathania D, Sharma S, Singh P (2013) Removal of methylene blue by adsorption onto activated carbon from *Ficus carica* bast. *Arabian Journal of Chemistry.*10:1445-1451. Doi.org/10.1016/j.arabjc.2013.04.021.

Peng Q, Liu M, Zheng J, Zhou C (2015) Adsorption of dyes in aqueous solutions by chitosan-halloysite nanotubes composite hydrogel beads. *Microporous Mesoporous Mater.* 201: 190-201.

Prasanth KVH, Tharanathan RN (2003) Studies on graft copolymerization of chitosan with synthetic monomers. *Carbohydr Polym* 54(3):43-51.

Puoci F, Iemma F, Spizzirri UG, Cirillo G, Curcio M, Picci N (2008) Polymer in Agriculture: a Review. *Am J Agric Biol Sci* 3(1):299–314. http://www.thescipub.com/abstract/?doi=ajabssp.2008.299.314.

Rabea EI, Badawy ME, Stevens CV, Smagghe G, Steurbaut W (2003) Chitosan as antimicrobial agent: applications and mode of action. *Biomacromolecules* 4: 1457–1465. https://doi.org/10.1021/bm034130m.

Rohindra DR, Nand AV, Khurma JR (2004) Swelling properties of chitosan hydrogels. South Pacific *J Nat Appl Sci* 22(1):32.

Salleh MAM, Mahmoud DK, Karim WA, Idris A (2011) Cationic and anionic dye adsorption by agricultural solid wastes: a comprehensive review. *Desalination* 280:1-13.

Shin HK, Park M, Chung YS, Kim HY, Jin FL, Choi HS, Park SJ, (2013) Preparation and characterization of chlorinated cross-linked chitosan/cotton knit for biomedical applications. *Macromol Res* 21: 1241–1246. https://doi.org/10.1007/s13233-013-1164-9.

Sluszny A, Silverstein MS, Kababya S, Schmidt A, Narkis M (2001) Novel Semi-IPN through vinyl silane polymerization and crosslinking within PVC films. *J Polym Sci Part A* 39: 8–22. https://doi.org/10.1002/1099-0518(20010101)39.

Sreńscek-Nazzal J, Narkiewicz U, Morawski AW, Wróbel R, Gęsikiewicz-Puchalska A and Michalkiewicz B (2015) Modification of Commercial Activated Carbons for CO2 Adsorption. *Acta Physica Polonica* A 129(3) DOI: 10.12693/APhysPolA.129.394.

Tabriz A, Alvi MAU, Niazi MBK, Batool M, Bhatti MF, Khan AL, Khan AU, Jamil T, Ahmad NM (2019) Quaternized trimethyl functionalized chitosan based antifungal membranes for drinking water treatment. *Carbohyd Polym* 207: 17–25. https://doi.org/10.1016/j.carbpol.2018.11.066.

Tan WF, Lu SJ, Liu F, Feng XH, He JZ, Koopal LK (2008) Determination of the Point of Zero Charge of Manganese Oxides with Different Methods Including an Improved Salt Titration Method. *Soil Sci* 173:277.

Travis CC, Etnier EL (1981) A survey of sorption relationships for reactive solutes in soil. *Journal of Environmental Quality* 10:8-17.

Venkata Ramana DK, Harikishore Kumar Reddy D, Yu JS, Seshaiah K (2012) Pigeon peas hulls waste as potential adsorbent for removal of Pb(II) and Ni(II)from water. *Chem Eng J* 197:24-33.

Verlee A, Mincke S, Stevens CV (2017) Recent developments in antibacterial and antifungal chitosan and its derivatives. *Carbohyd Polym* 164: 268–283. https://doi.org/10.1016/j.carbpol.2017.02.001.

Vinh T, Duckshin P, Young-Chul L (2018) Hydrogel applications for adsorption of contaminants in water and wastewater treatment. *Environmental Science and Pollution Research* 25(25): 24569-24599 DOI 10.1007/s11356-018-2605-y.

Wen Y, Yao FL, Sun F, Tan ZL, Tian L, Xie L., et al., (2015) Antibacterial action mode of quaternized carboxymethyl chitosan/poly(amidoamine) dendrimer core-shell nanoparticles against Escherichia coli correlated with molecular chain conformation. *Mater Sci Eng C* 48: 220–227. https://doi.org/doi:10.1016/j.msec.2014.11.066.

Wu FC, Liu BL, Wu KT, Tseng RL (2010) A new linear form analysis of Redlich-Peterson isotherm equation for the adsorption of dyes. *Chemical Engineering Journal* 162:21-27.

Xin Z, Du S, Zhao C, Chen H, Sun M, Yan S, et. al (2016) Antibacterial performance of polypropylene nonwoven fabric wound dressing surfaces containing passive and active components. *Appl Surf Sci* 365:99-107.

Yan T, Li C, Ouyang Q, Zhang D, Zhong Q, Li P, Li S, Yang Z, Wang T, Zhao Q (2019) Synthesis of gentamicin-grafted-chitosan with improved solubility and antibacterial activity. *React Funct Polym* 137:38–45. https://doi.org/10.1016/j.reactfunctpolym.2019.01.013.

Ye B, Meng L, Li Z, Li R, Li L, Lu L, et al. (2016) A facile method to prepare polysaccharide-based in-situ formable hydrogels with antibacterial ability. *Mater Lett* 183:81–84.

Yeul VS, Rayalu SS (2013) *J Polym Environ* 21(2):606–614.

Yilmaz E (2004) Chitosan: A Versatile Biomaterial. *Biomaterials.* 553:59-68.

You R, Xiao C, Zhang L, Dong Y (2015) Versatile particles from water-soluble chitosan and sodium alginate for loading toxic or bioactive substance. *Int J Biol Macromol* 79: 498-503.

Yu Z, Liu W, Huo P (2019) Preparation, characterization, and antimicrobial activity of poly(γ-glutamic acid)/chitosan blends. *Polym Bull* 76:2163–2178. https://doi.org/10.1007/s00289-018-2485-9.

Zhao L, Mitomo H, (2008) Adsorption of heavy metal ions from aqueous solution onto chitosan entrapped CM-cellulose hydrogels synthesized by irradiation. *Journal of Applied Polymer Science. 110(3)*: 1388-1395. https:// doi.org/10.1002/app.28718.